GEMINI
8-M Telescopes
Project

RPT-C-G0049

Tip-Tilt Chopper Control Study and Power Requirements

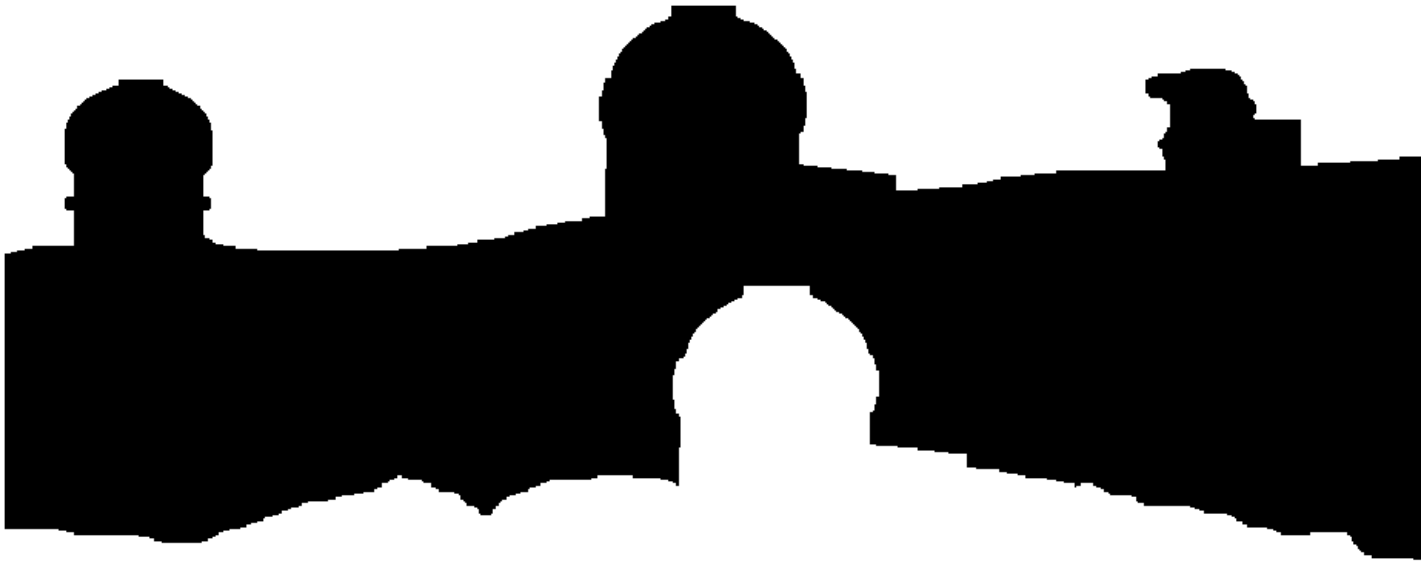

M. Burns
Controls Group

March 22, 1993

GEMINI PROJECT OFFICE 950 N. Cherry Ave. Tucson, Arizona 85719
Phone: (520) 318-8545 Fax: (520) 318-8590

GEMINI 8-METRE TELESCOPES PROJECT
CONTROLS GROUP

To: File

Copied To: R. McGonegal

From: Mike Burns

Date: March 22, 1993

Subject: Tip-Tilt Chopper Control Study and Power Requirements

Reference: Power Requirements for Chopper, R. McGonegal, January 17, 1993.

Problem

It is required that the chopping secondary servo system provide 56.4 arcsecond (=270 micro-rad) motion at a rate of 10Hz. The required settling band of 0.485 micro-rad must be reached in 0.01 seconds to provide a usable duty-cycle of 80%.

A candidate controller is developed which meets the requirements and the resulting model is used to estimate the average power.

Summary

- digital control looks very troublesome at 200 Hz sampling
- need 1kHz or more sampling to try digital
- continuous control needs 640Hz bandwidth estimator and 75 W net power
- summary of power and duty-cycle for various controllers:

Controller type	Power- 1 actuator (W)	Net Power (W)	Duty-Cycle (%)
Original PID-Benign	5	8	80
Original PID-parasitics	20	30	72
PID-increased gain	32	48	79
Digital PID	3	4	0
Kalman filter/Optimal ctrl	50	75	88

System Model

The basic model of the servo-chopper system is nearly the same as that described in the reference with the addition of some parasitic terms. The calculations of torque and power also have been changed slightly.

Figure 1 shows the generalized top-level view of the simulation used for this study. Input is

modeled as a 270 micro-rad step that is subtracted from the actual angular position of the secondary to produce an error, labeled Theta-err. The controller block, expanded in Figure 2, acts upon the error to produce a limited command voltage, Vlim, which feeds the servo block of Figure 3. The servo block produces Torque delivered to the Chopper of Figure 4 and an intermediate variable, Ilim, the limited current used by the Power block of Figure 5.

The overall simulation is "mixed" in the sense that part of the simulation describes a single actuator and part of the simulation describes the summed effect of 3 actuators. The Controller, Servo, and Power blocks model one actuator, while the Chopper block models the effects of all 3 actuators. The crossover from part to whole occurs in the last gain block of the servo, Figure 3, which is labeled i2trq. The gain i2trq is the scale factor from current in one actuator to net torque produced by 3 actuators.

Figure 6 helps to describe the relationship i2trq. Assume that the 3 actuators are placed in the geometry shown and produce forces labeled F1, F2, and F3 Newtons. The desired rotational axis is labeled xx' and the moment arm is z=0.3 meters. The fact that torque is about the xx' axis requires that

$$F2 = F3.$$

Net force on the mirror must balance, requiring that

$$F1 + F2 + F3 = 0.$$

Combining the above 2 equations gives

$$F2 = F3 = -F1 / 2.$$

Noting that sin(30 deg)=0.5, the diagram makes it clear that net torque will be

$$Tnet = F1*z - F2*z/2 - F3*z/2 \quad \text{or}$$

$$Tnet = F1*z + F1*z/4 + F1*z/4$$

$$Tnet = F1*z*3/2.$$

For this possible actuator, the relationship between current and force is 35N/A, so the previous equation can be written

$$Tnet = I1 * 35N/A * 0.3m * 3/2 = I1 * 15.8,$$

showing that the gain i2trq=15.8N*m/A. This is half the value used in the reference but is believed to be more accurate. By way of an argument similar to the one above, the net power may be shown to be 1.5 times the power in the actuator number 1.

Note that an alternate geometry would be to draw the axis of rotation through one of the

actuators in Figure 6. It is not shown here, but the resulting i2trq=18.2. The 15.8 value is chosen because it is the more pessimistic (hitting the current-limit and torque-limit sooner). In general, the geometry would influence controller gains between these extremes.

The Servo block of Figure 3 also shows two other small changes from the referenced memo: addition of a back-EMF term and an electrical time constant, taue=0.25 milli-seconds.

A first guess at the controller model is to use the PID controller of the reference. Note that gains appear doubled because this controller goes from theta-err to volts, whereas the reference went from theta-err to current. Current and voltage are related by the 2 ohm armature resistance. The derivative term of the controller is changed from a pure differentiator to one with a very small time-constant, taud=0.3ms to reflect the lag inherent in measuring or calculating speed. The controller also includes a voltage limiter which was not modeled in the reference, but is always part of a power amplifier which will drive the servo. Note that the current limit is also modeled, but is not sufficient. Roughly, the current limit restricts net force and voltage limit restricts rate of change of force.

The chopper of figure 4 is fundamentally unchanged from the reference, and the Power block integrates I*I*R and divides by the 0.05sec half-wave time to get average power.

To summarize, the basic model used in this study is the same as that of the referenced memo except for the following changes:

- i2trq changed from 31.5 to 15.8 N/A
- voltage limiting
- back EMF in servo
- servo dynamic time constant of taue=0.25 ms
- controller differentiator time constant, taud=0.3 msec.

SIMULATION RESULTS AND THE SEARCH FOR A GOOD CONTROLLER

Original PID-Benign case

Figure 7 shows simulation results for the most benign possible case, omitting voltage limiting, omitting back EMF, omitting servo electrical time-constant, and having negligible (0.03 ms) differentiator time-constant. The measured outputs are from top to bottom: Theta-error (rad), servo voltage (V), servo current (A), mirror angle (rad), angular rate (rad/sec), and average power (W). Figure 8 redraws the error on a better scale and shows that the spec is met since error falls below 0.485 micro-rad before 0.01 sec. Despite the integral term, the MatrixX implementation of this PID controller has a non-zero steady state error. This error is likely due to quantization effects within MatrixX or to the very tiny integral gain which causes an error to be reduced only very slowly. The resulting power is 5.1 W.

Original PID-with parasitics

Figures 9 through 18 show the effects of adding gradually more of the parasitic effects. The voltage limit and back-EMF have little effect on power, perhaps reducing power marginally, and make the system slightly slower such that the 0.485 micro-rad settling band is not reached until 0.012 sec. The addition of an electrical time-constant has increases power consumption 40% to 7 W. The most devastating effect upon power comes from the controller differentiator lag, taud. Increasing it to 0.1 ms then to 0.3 ms increases power to 9.5 W and 20W. If taud is increased to 1ms, the controller is hopeless, with power increasing to 65W and settling time going to 0.04 sec. Taud=0.3 ms was chosen rather arbitrarily as a good representative value of a realistic sensor without greatly harming performance.

PID-increased gain

Can the structure of this controller be saved and adequate performance restored by changing gains? The root locus plots of Figures 19-24 help in describing this system. The first 3 of these figures show the root locations of the benign system for changing the proportional, integral, and derivative gains by the scale factors shown on the plots. It is interesting to note that the integral gain may be changed by a factor of 20 while moving the root location negligibly. This indicates that the original controller was nearly a PD type. Since the derivative time constant, taud, was the most important of the parasitic elements modeled, its root locus is shown in Figure 22. Predictably, things get much slower for taud=0.3 ms than for 0.03 ms. Figures 23 and 24 show the proportional and derivative root loci again, this time for the less benign case of taud=0.3 ms. Increasing either the P or D gain improves the root on the real axis near -400 at the expense of the lightly damped root near 400 +j1600. Increasing the P gain by a factor of 1.5 seems to give the best tradeoff, with time responses shown in Figures 25 and 26. The settling time has been restored to near 0.0105 sec but power has increased to near 32 W.

Digital control

Thus far only a continuous time controller has been modeled, but in the actual system there are strong reasons for using a digital controller, notably ease in changing parameters and stability of

coefficients. Figure 27 shows the root locus of the discretized system with a 200Hz sampling rate and an extra step delay to represent computational lag. Figure 27 was found to be poor because of the root near -0.8 at the left of the plot tending to go unstable as gain increased. Figure 28 shows the effect of adding a lead-lag compensator to pull in the errant pole. Still the system response of Figure 29 is poor. Note that at 200Hz the controller has precisely 2 steps in which to reduce the system error by a factor of 0.0018 (from 270 to 0.485 micro-rad), so the effective system root must be near sqrt(0.0018)=0.04 . This is so close to deadbeat as to likely be unattainable with a linear controller, so a bang-bang type controller was examined for the first two steps handing off to a slower linear controller to maintain good noise response.

Figure 30 shows the MatrixX block diagram of a controller which was cascaded with the linear digital controller to implement the bang-bang function over the first two time steps. The bang-bang control used here is slightly more sophisticated than that described in the reference in that the chopper is modeled as inertia-spring-damper rather than merely inertia. Following are a few words about derivation of the control steps.

The chopper may be represented by the discrete state space equation

$$x(k+1) = PHI * x(k) + gam * u(k)$$

where x(k) is the state [theta(rad) theta-dot(rad/sec)]' and u(k) is the applied torque. It is desired to find torques u(0) and u(1) such that the system is moved from its original state x=[0 0]' to the state [2.7e-4 0]' . The state space equation may be iterated to give

$$x(1) = PHI * x(0) + gam * u(0)$$

$$x(2) = PHI * PHI * x(0) + PHI * gam * u(0) + gam * u(1) .$$

The last equation above is a simple linear equation in the unknowns u(0) and u(1) and may be rearranged and solved:

$$x(2) = PHI * PHI * x(0) + [PHI * gam \mid gam] * [u(0) \ u(1)]' \quad \text{or}$$

$$inv[PHI * gam \mid gam] * [x(2) - PHI*PHI*x(0)] = [u(0) \ u(1)] \ .$$

Solving the above gives the necessary step torques of u(0)=43.618 Nm and u(1)=-41.321Nm. This is quite close to the simpler values derived in the reference of +/- 43.68 Nm, showing that inertia is much the dominant term. Neglecting the effect of the electrical time constant, the computed torques correspond to commanded voltages of 5.521V and -5.231V respectively. Unfortunately, when these are applied to the system the effect is completely unsatisfactory as shown in Figure 31. The large transient response in theta-err is due to the neglected state associated with the electrical time constant. Figure 32 verifies that the system response is excellent, with theta-err=0.03 micro-rad, when the electrical lag is removed. One could rewrite the state equations to include the effect of the electrical lag, but it would require at least 3 time steps to move all three states to the arbitrary location, violating the 0.01 sec required settling time.

In general an N-state system will require N steps to move from one state to another specified state. Even if we were to build a controller that would take into account the known states, unmodelled states would remain which would cause harm analogous to that shown above. One would still need a fast linear controller to take out the system error. For example, with a 1kHz sampling rate, one would have 10 steps in which to remove error. The first 3 steps could be used to take out the 3 known states and the other 7 steps could remove the remaining error due to unmodelled effects. Due to actuator current limit, and thus torque limit, 3 steps might be insufficient time in which to move the system. In such a case more steps could be used or the effective torque limit could be increased by including 4 or more actuators in a different geometry.

A 1kHz digital filter should easily be implementable on the current system. For an n-state filter, there are required roughly n^2+3n floating point multiplies and as many floating point adds. So a 5 state filter would need approximately 40 multiplies and 40 adds. Assuming a 68030 processor operating at 25MHz, there are 25,000 clock cycles in a 1ms sample time. Conservatively estimating that a floating point multiply takes 64 clock cycles and an add takes 44 clock cycles gives a total of 4,000 clock cycles for the filter. Doubling this to 8,000 clock cycles to conservatively estimate the necessary software overhead still uses only 1/3 of the available CPU power.

Kalman Filtering/Optimal Control

Since the above analysis shows that a 200Hz digital system has little hope of working, a Kalman-filtering/optimal-control type approach was considered in the continuous domain. Figure 33 shows the resulting system with the estimated states being chopper-angle, angle-rate, and servo-current. Properly speaking, the system shown is neither Kalman-filtering nor optimal-control because the estimator gains ke and controller gains kc are not chosen based on measurement or system noise. Still, the structure is the same. Figures 34 and 35 show the time responses associated with the first iteration of this approach, with controller gains which give poles at -1000 and -700 +/-j714 and estimator gains which give poles at -2000 and -1400 +/-j1428. The transient response is seen to die out quickly enough in 6 ms, but there is left a steady-state error of 1 micro-rad, well above the specified 0.485 micro-rad. One alternative is to add another state, integrated error, and redo the filter and controller gains for the resulting 4-state system. A more simple approach was taken in just making the controller stronger. Figures 36 and 37 show the effect of moving the controller poles to -2000 and -1400 +/-j1428 and the estimator poles to -4000 and -2800 +/-j2828. Now the steady-state error is only 0.25 micro-rad. If this steady-state error were unacceptable, one could cascade the limited PI controller of figure 38. The limiter before the integrator insures that it will not become highly charged by the initial violent transient and will only affect the long term response as shown in Figures 39 and 40. The estimator pole at -4000 rad/sec is equivalent to a bandwidth of 640Hz which should easily be implementable.

Notes on Scaling

All of the controllers presented here are likely to have a much easier time at a slower chopping rate. Since every controller has an initial transient response similar to bang-bang, it seems

reasonable to consider the equation from the reference:

T^2 = 4 * theta * J / torq

where T is the travel time, theta the angle to be traversed, J the moment of inertia, and torq the maximum torq. Assuming that most of the power is used in the initial transient and letting "~" represent "is proportional to" the following dependencies are noted:

Pav ~ Pmax ~ current^2 ~ torq^2 ~ 1/T^4 ~ theta^2 .

So for example with a 5Hz chopping rate and a 540 micro-rad angle, the net effect is that power is reduced by a factor of 4. Note that this assumes that the torq limit (current limit) is similarly reduced for the slower chopping case. For those controllers which meet the required settling time this would be allowable. The response could be speeded up by allowing a comparatively larger torque limit at the expense of more power, offering hope for some of the slower controllers which barely missed meeting the settling time.

Future Work Possibilities

- examine plant and measurement noise effect on Kalman filter approach
- model power amplifier dynamics, possibly including a state in the estimator
- find effect of reaction force (torque doublet) on structure
- find tracking bandwidth and residual error spectra of resulting closed loop system
- look at the effect of Coulomb friction upon tracking accuracy and power
- test robustness to modeling errors such as chopper spring constant
- consider a digital controller at higher sampling rate and a 5-state estimator to model
- computational lag, amplifier dynamics, and electrical lag

Figure 1

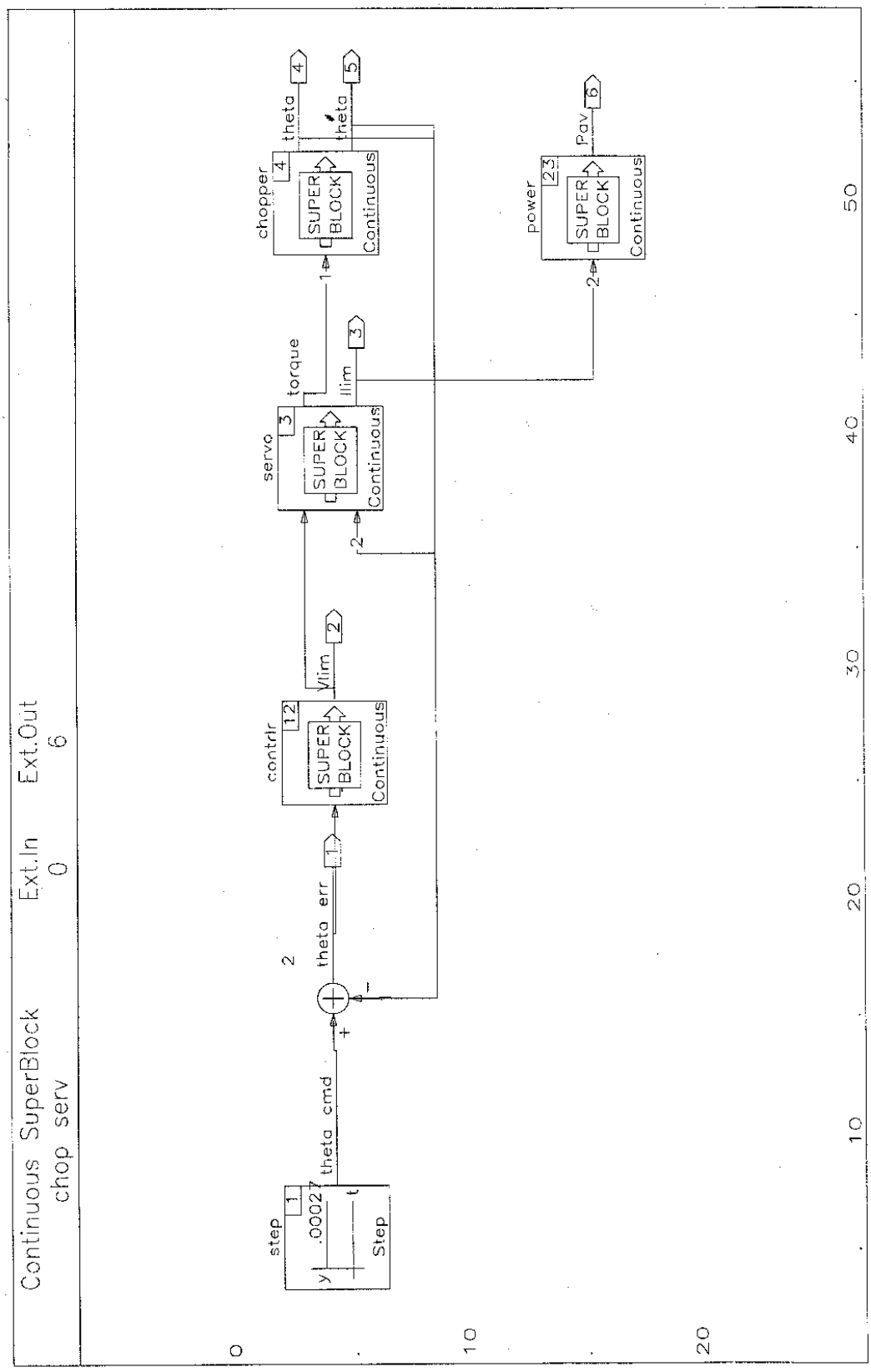
Continuous SuperBlock
chop serv
Ext.In
0
Ext.Out
6
step
.0002
Step
theta cmd
theta err
contlr
SUPER BLOCK
Continuous
Vlim
servo
torque
Ilim
chopper
theta
power
Pav
0
10
20
30
40
50

Figure 2

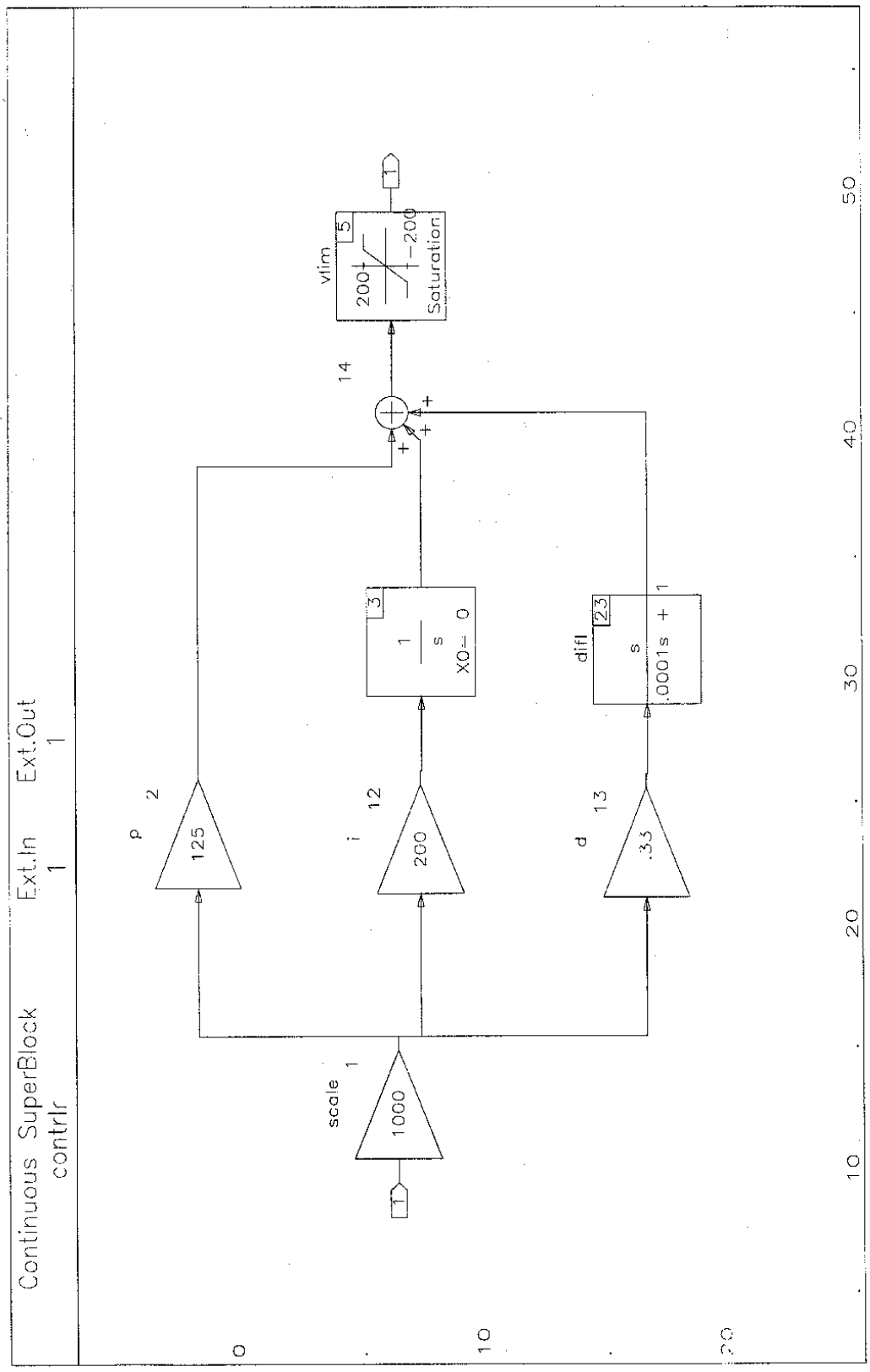
Continuous SuperBlock
contrlr
Ext.In 1
Ext.Out 1
vlim
5
200
-200
Saturation
14
3
1
s
X0= 0
difl
23
s
.0001s + 1
p 2
125
i 12
200
d 13
.33
scale 1
1000
1
1
0
10
20
30
40
50

Figure 3

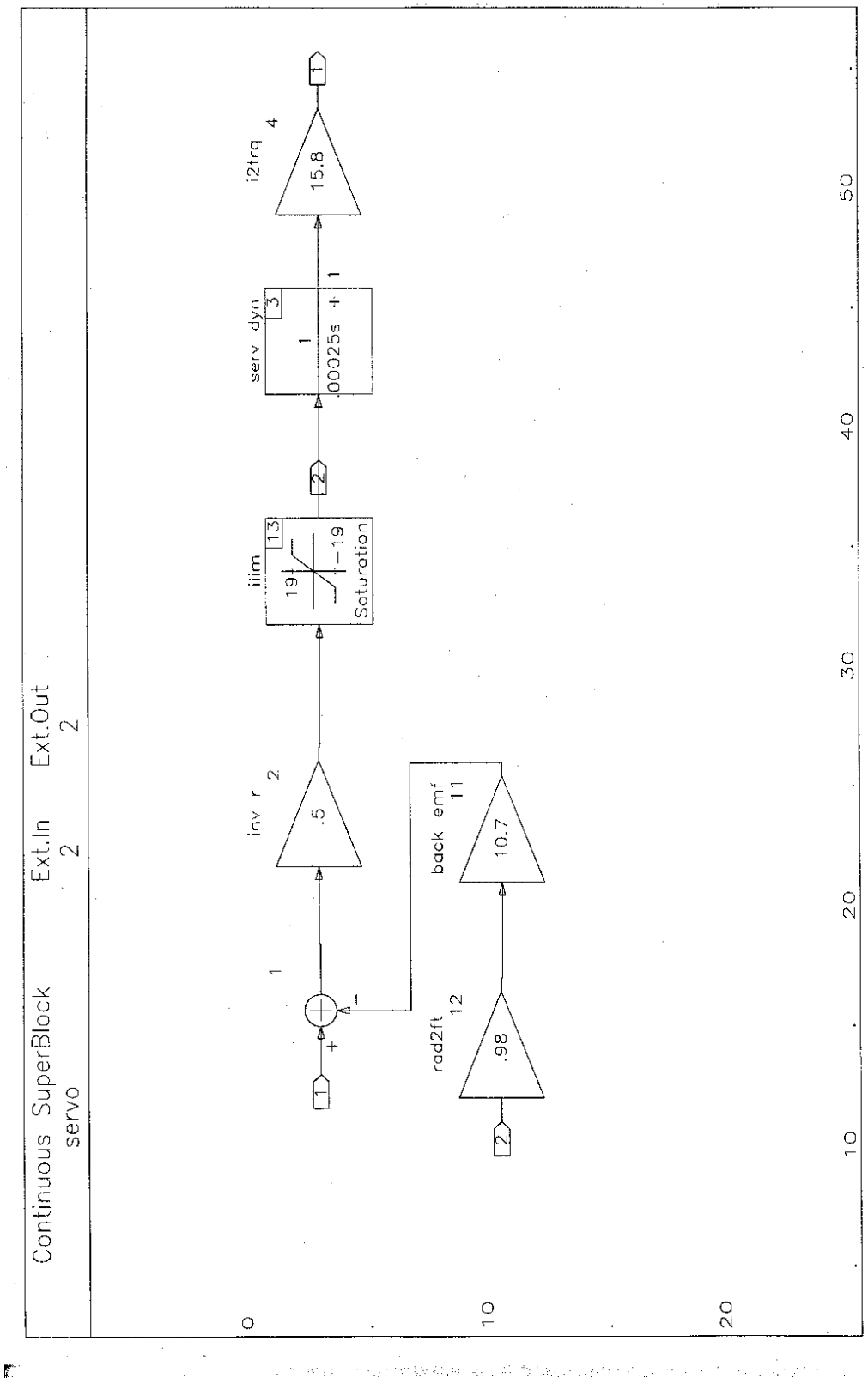
Continuous SuperBlock
servo
Ext.In 2
Ext.Out 2
i2trq 4
15.8
serv dyn 3
1
.00025s + 1
ilim 13
19
-19
Saturation
inv r 2
.5
back emf 11
10.7
rad2ft 12
.98
1
2
+
-
0
10
20
30
40
50

Figure 4

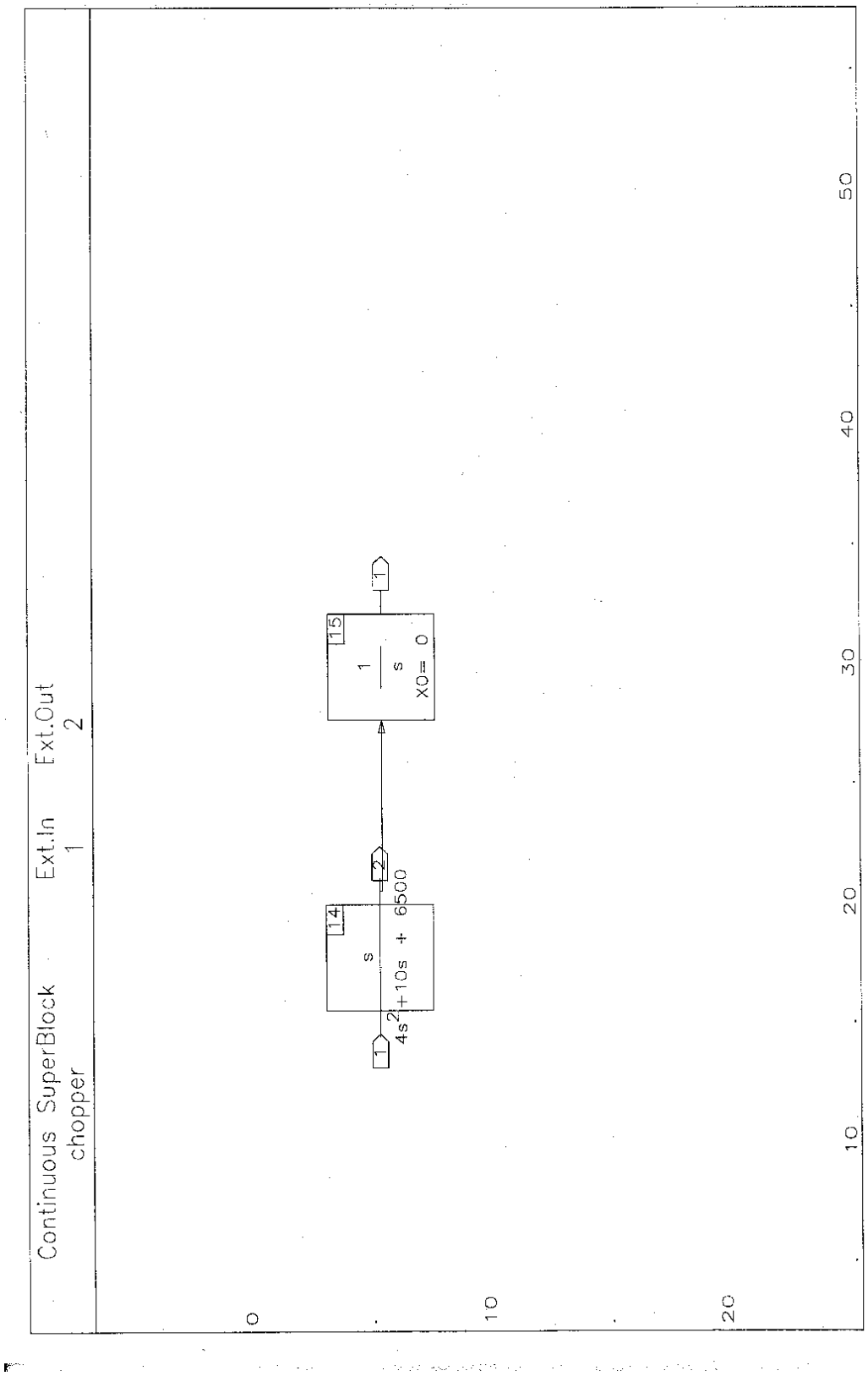
Continuous SuperBlock
chopper
Ext.In 1
Ext.Out 2
14
s
4s2+10s + 6500
15
1
s
X0= 0
1
2
1
0
10
20
10
20
30
40
50

Figure 5

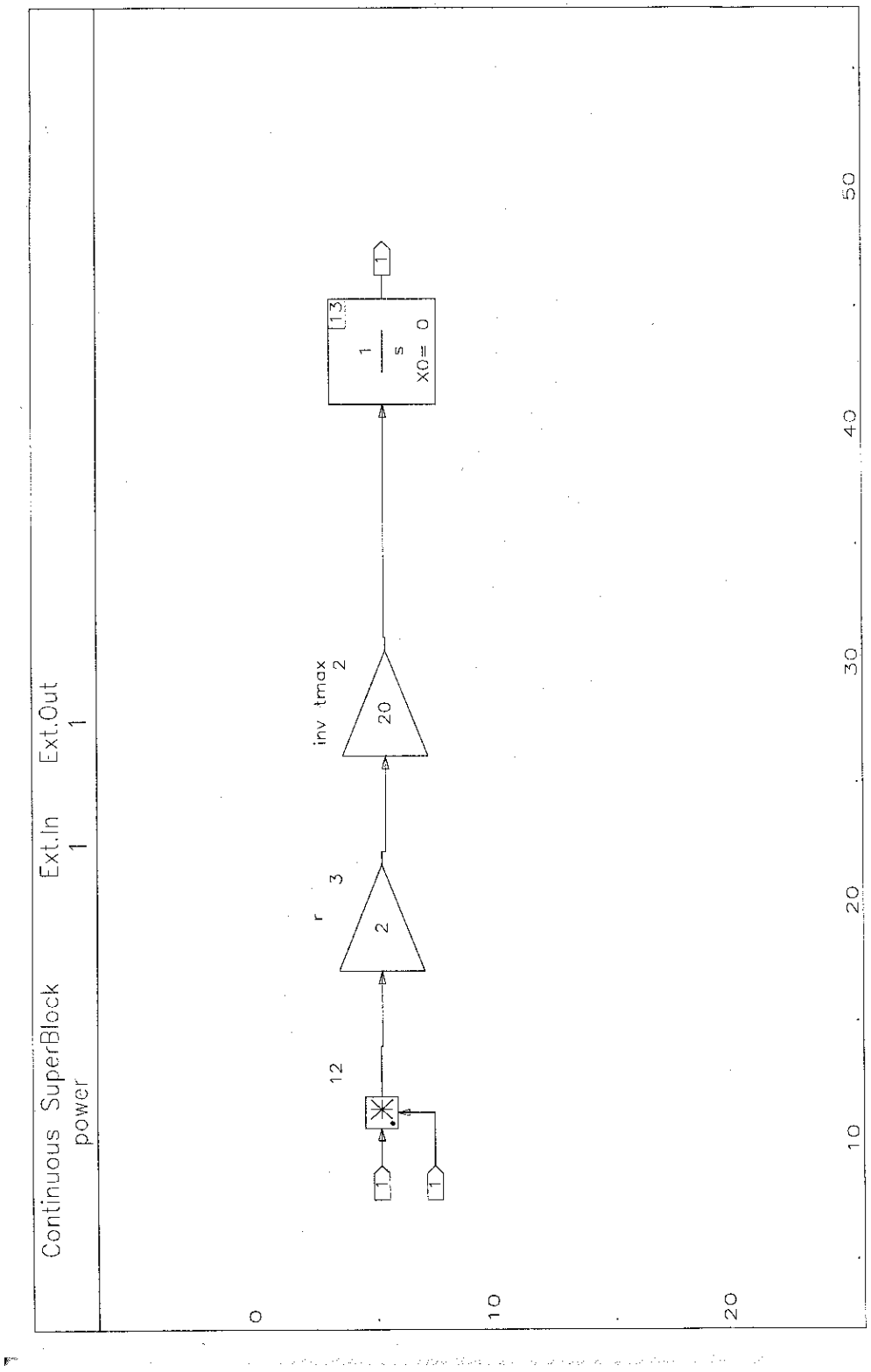
Continuous SuperBlock
power
Ext.In
1
Ext.Out
1
1
13
1
s
X0= 0
inv tmax
2
20
r
3
2
12
1
1
0
10
20
10
20
30
40
50

Figure 7

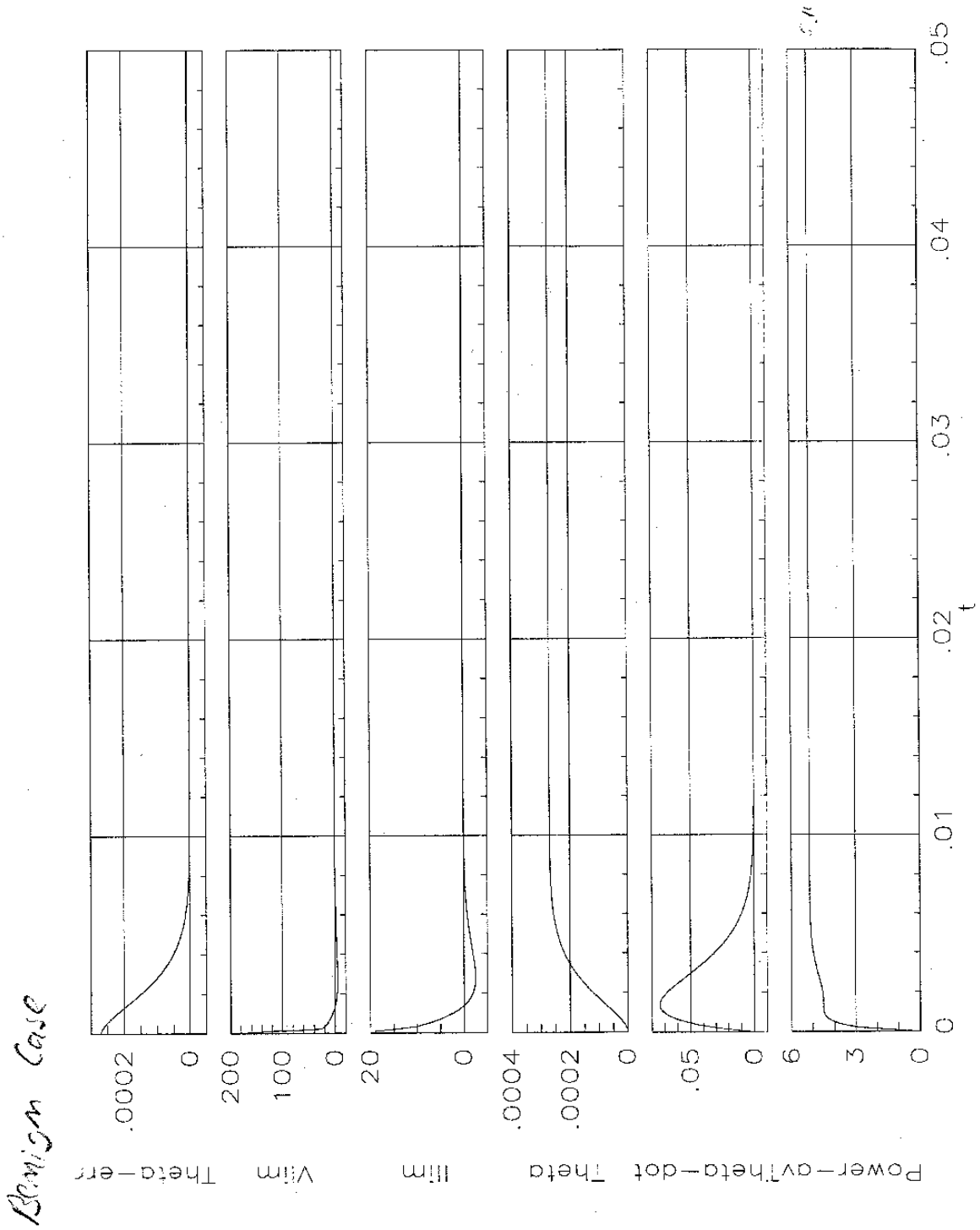
Power−gv7theta−dot
Theta
iim
Vlim
Theta−err
.0004
.0002
0
.05
0
6
3
0
200
100
0
20
0
.0002
0
0
.01
.02
.03
.04
.05
t

Figure 8

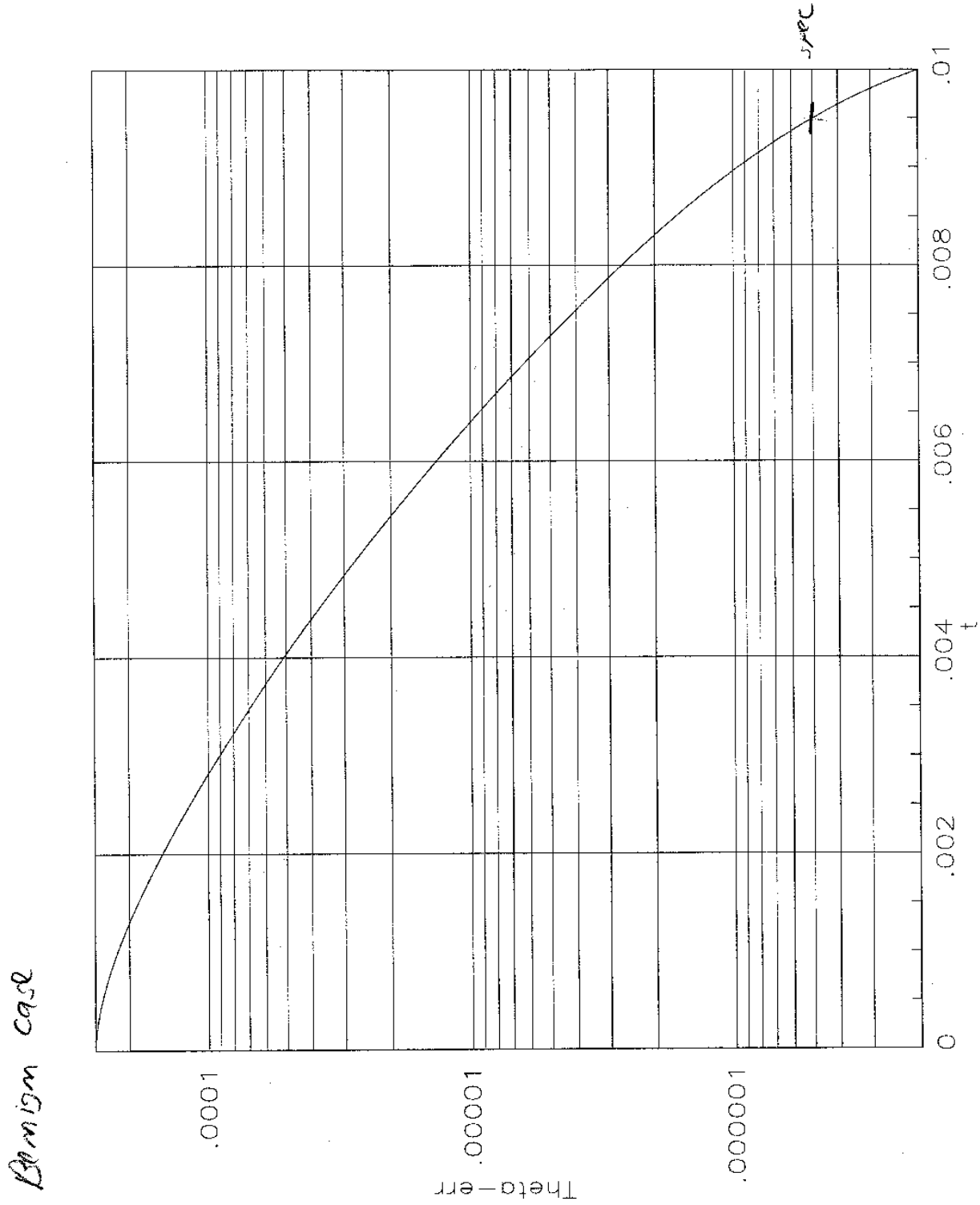

Figure 9

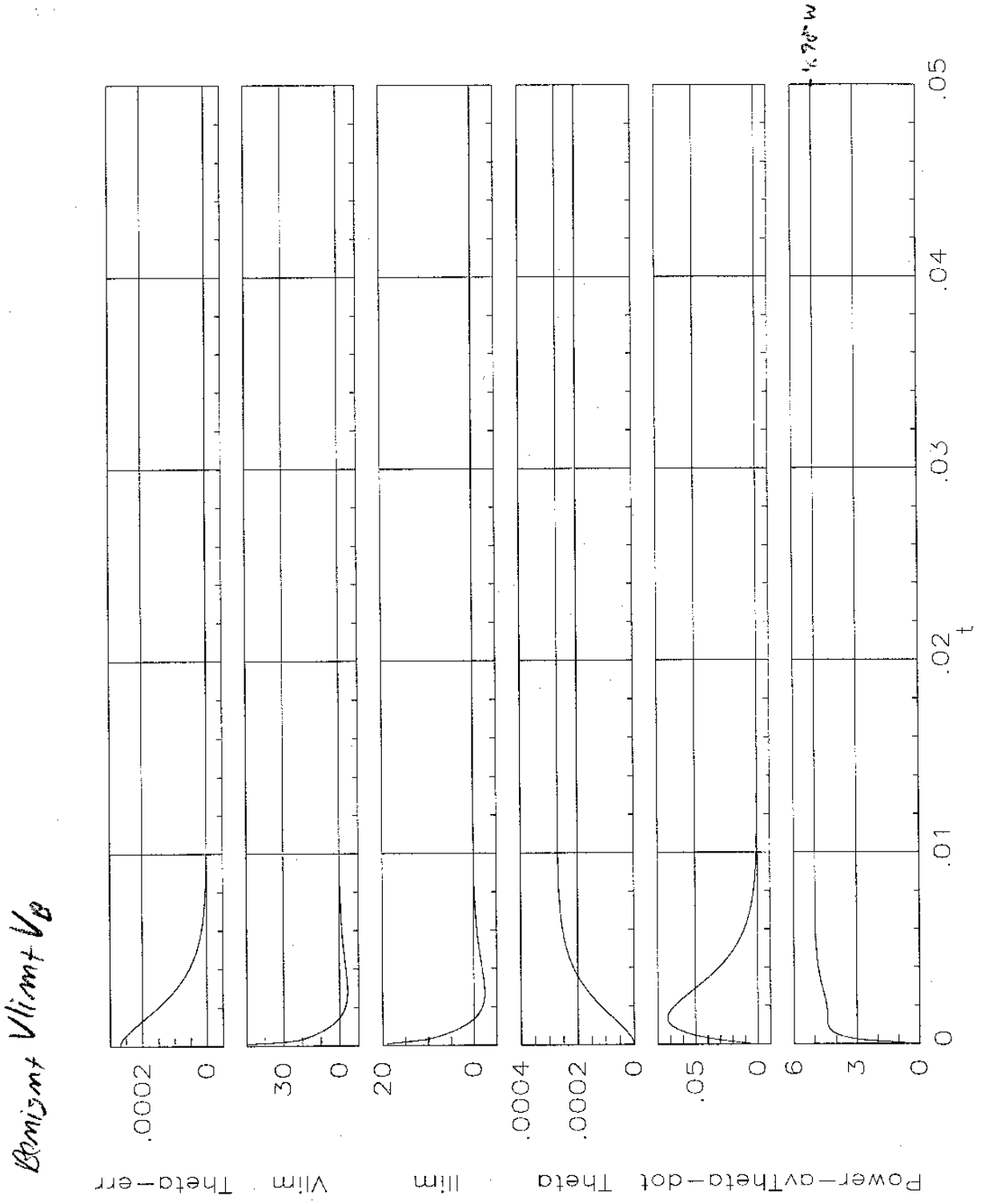
Power
avTheta-dot
Theta
Vlim
Theta-err
.0004
.0002
0
.05
0
6
3
0
30
0
20
0
.0002
0
.01
.02
.03
.04
.05
t

Figure 10

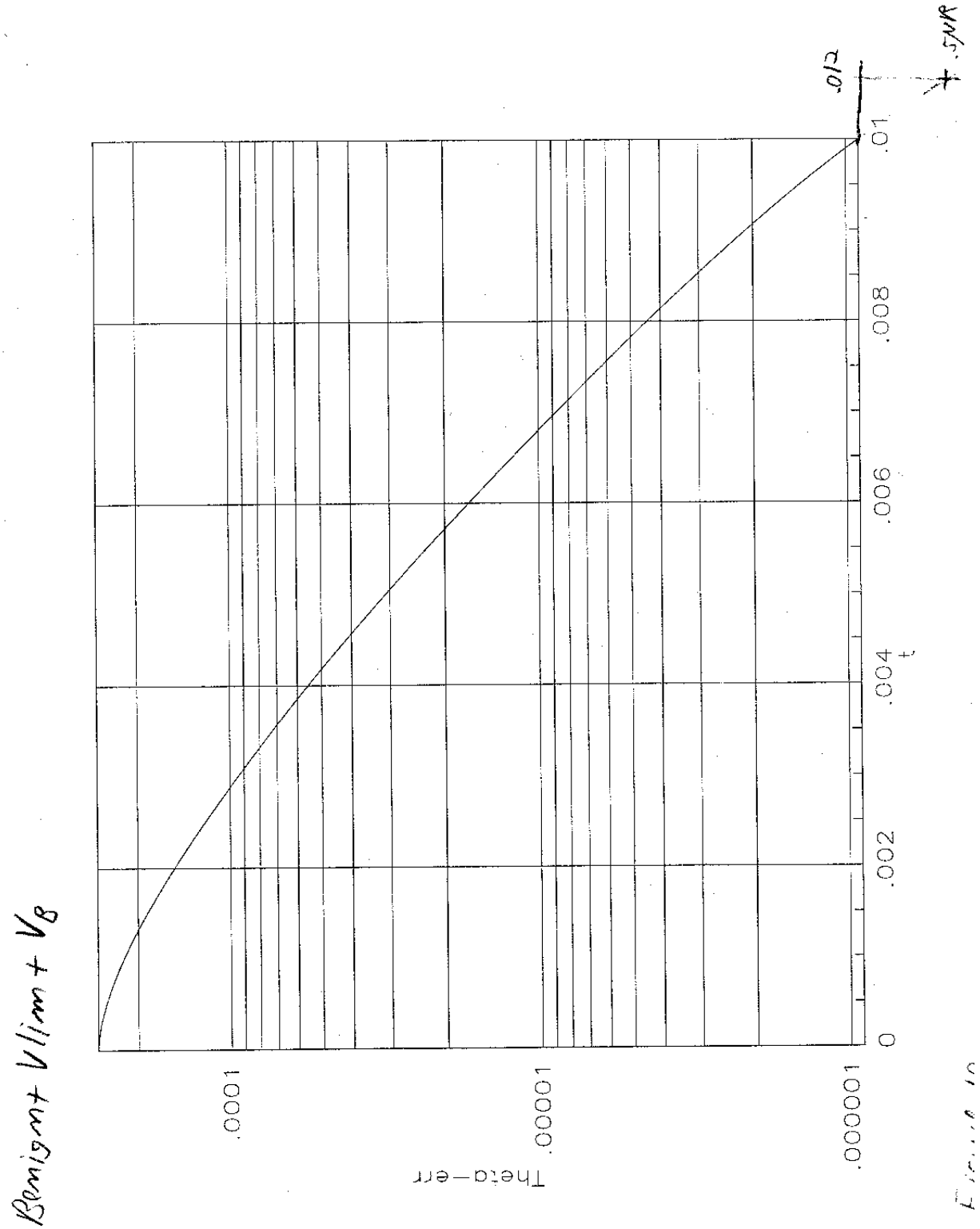

Figure 11

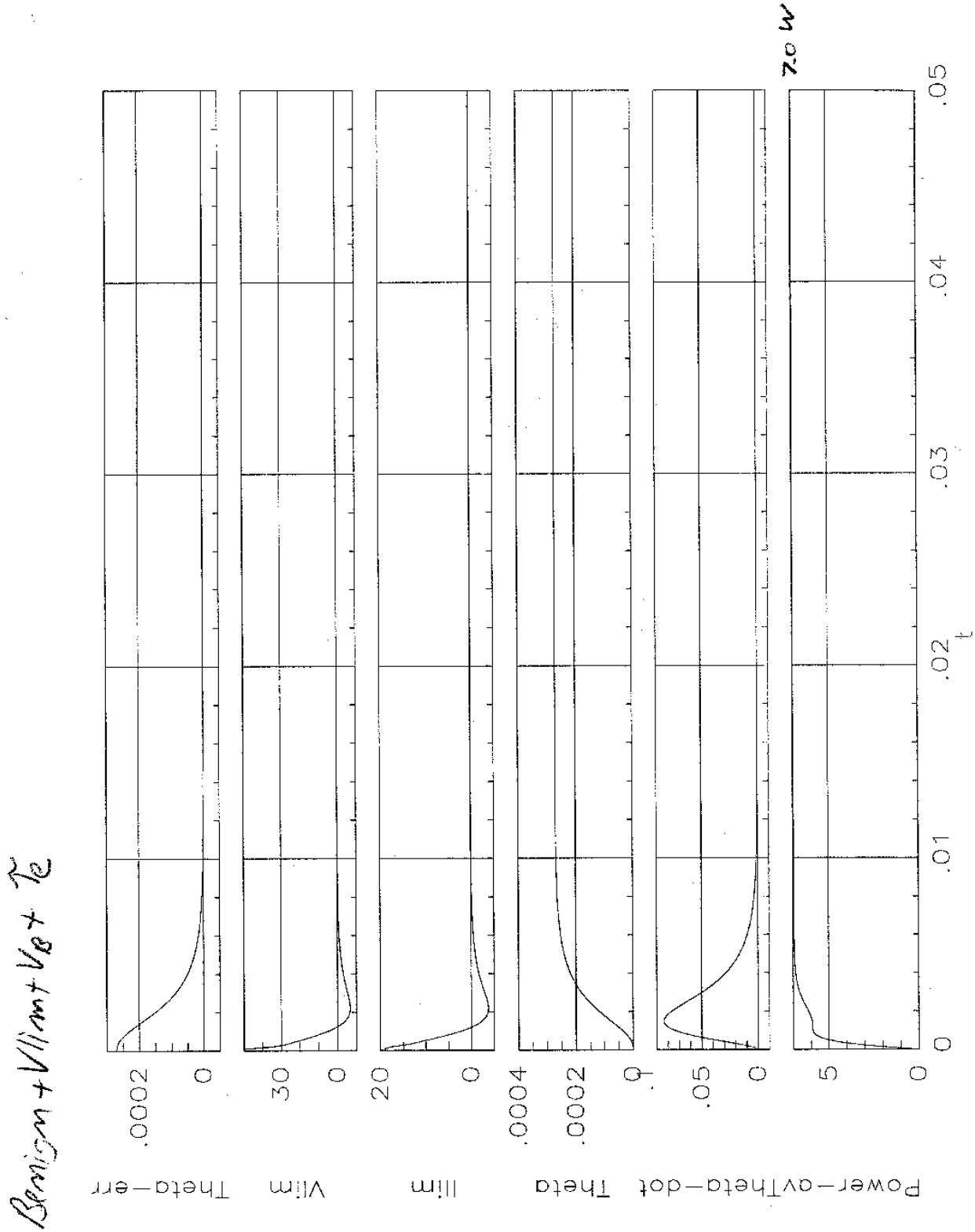
Power
ovTheta_dot
Theta
Iim
Vim
Theta_err
t
.05
.04
.03
.02
.01
0
.0002
.0004
20
30
5
.1
.05

Figure 12

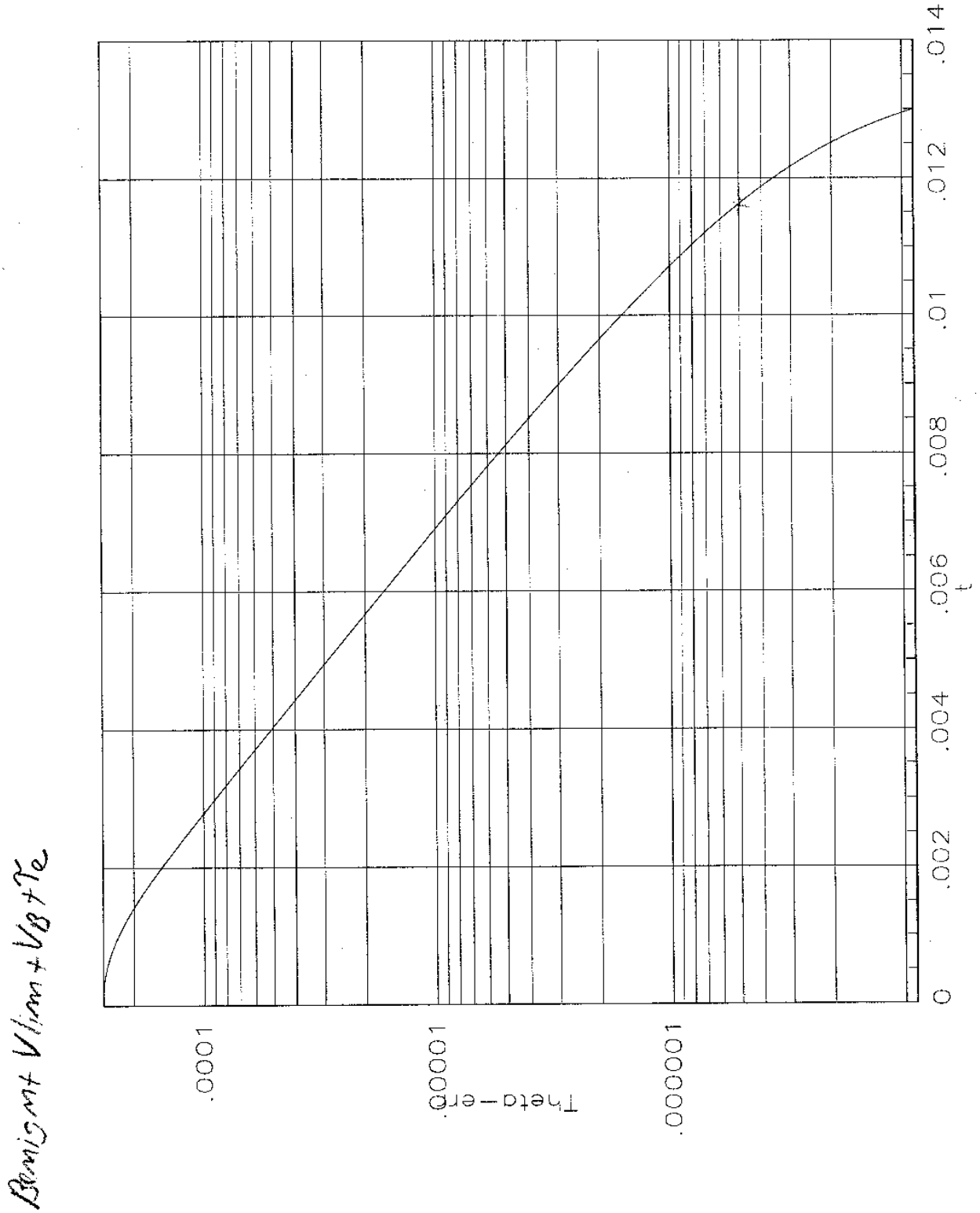
Ramicmt Vlim + VB + Te
Theta-err
.0001
.00001
.000001
0
.002
.004
.006
.008
.01
.012
.014
t

Figure 13

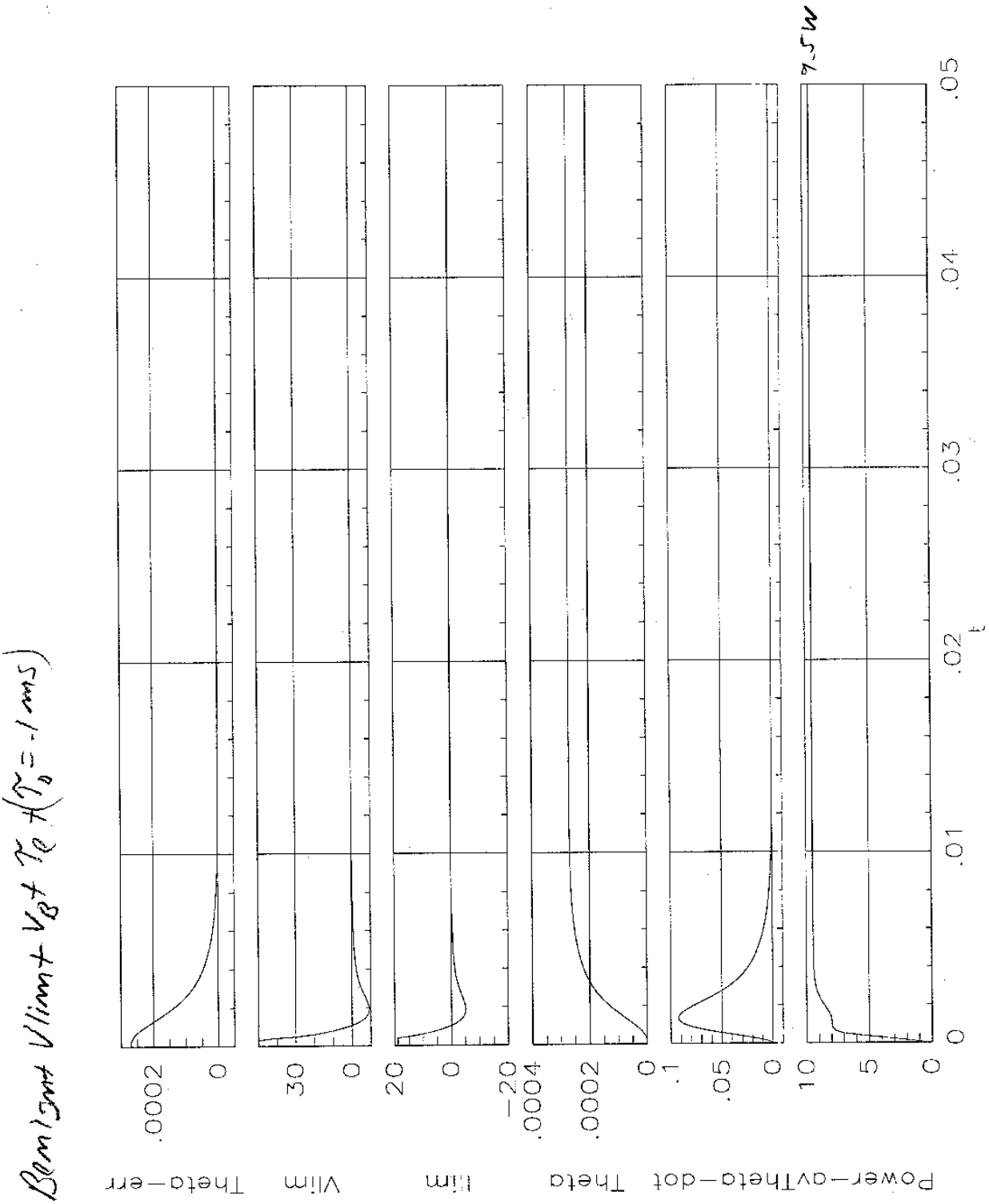
Power
avTheta-dot
Theta
Ilim
Vlim
Theta-err
.0002
0
30
0
20
0
-20
.0004
.0002
0
.1
.05
0
10
5
0
0
.01
.02
.03
.04
.05
t

Figure 14

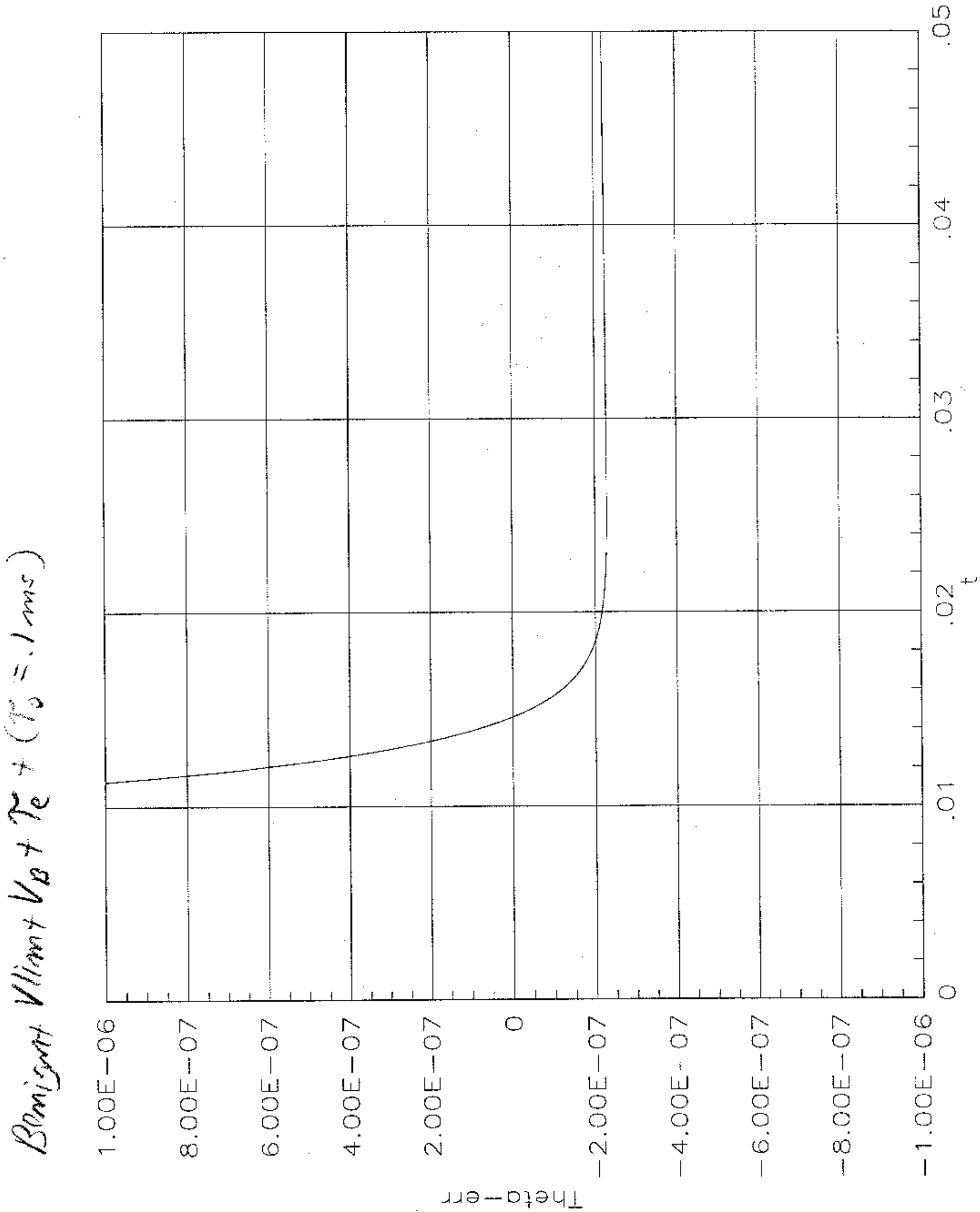
1.00E−06
8.00E−07
6.00E−07
4.00E−07
2.00E−07
0
−2.00E−07
−4.00E−07
−6.00E−07
−8.00E−07
−1.00E−06
Theta—err
0
.01
.02
.03
.04
.05
t

Figure 15

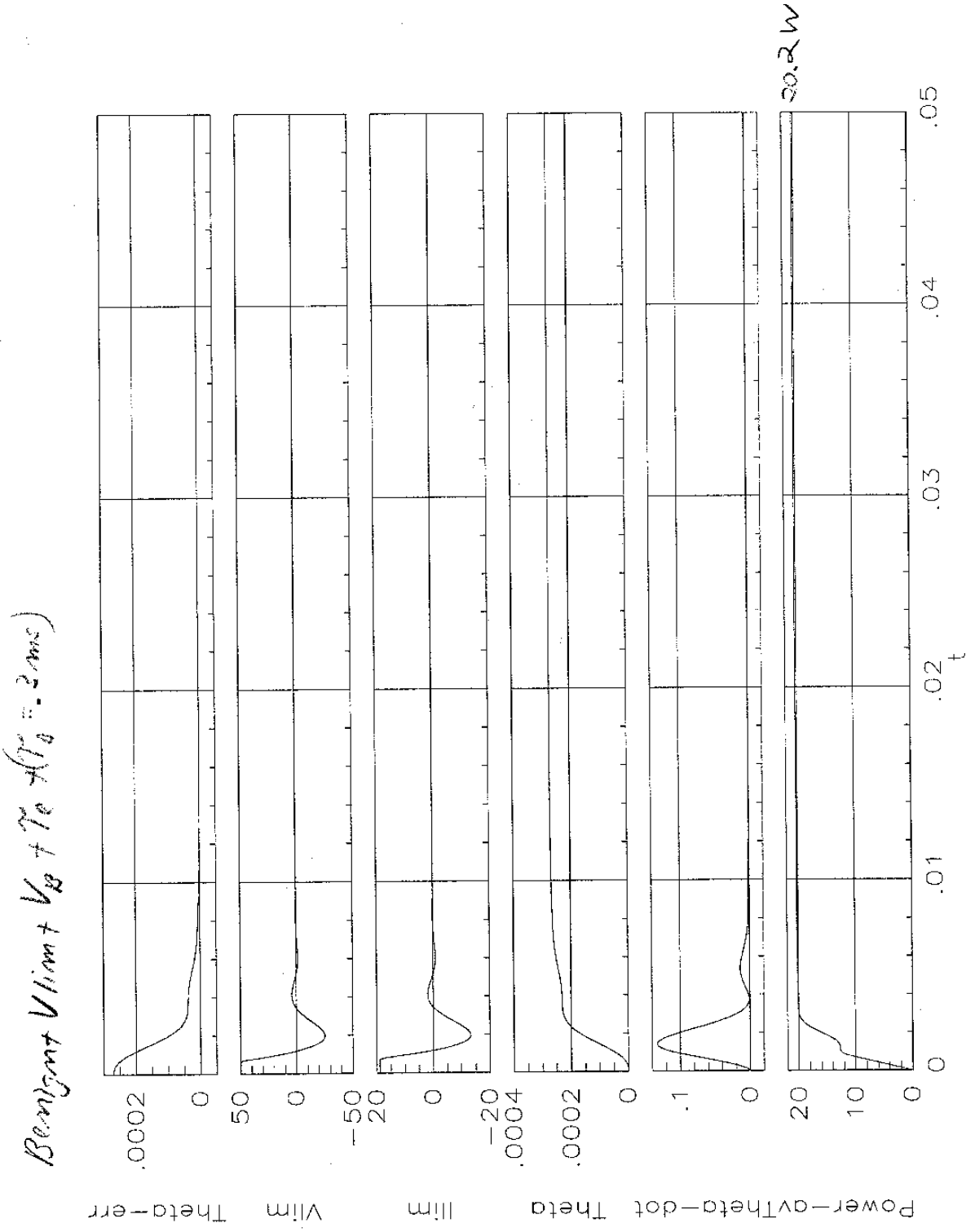
Power
avTheta-dot
Theta
Ilim
Vlim
Theta-err
20.2 W
t
0
.01
.02
.03
.04
.05
.0002
0
50
0
-50
-20
0
-20
.0004
.0002
0
.1
0
20
10
0

Figure 16

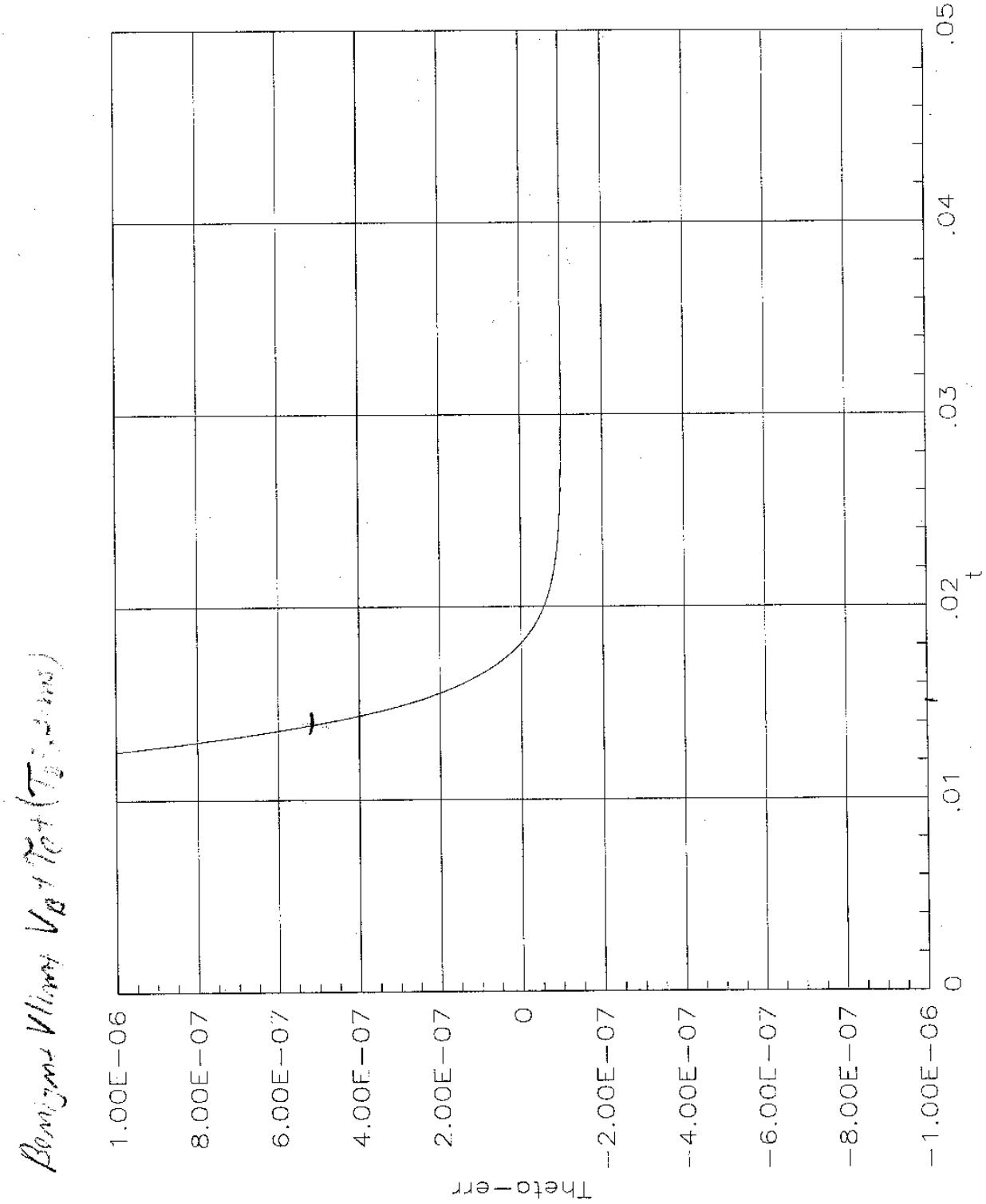
1.00E−06
8.00E−07
6.00E−07
4.00E−07
2.00E−07
0
−2.00E−07
−4.00E−07
−6.00E−07
−8.00E−07
−1.00E−06
Theta−err
0
.01
.02
.03
.04
.05
t

Figure 17

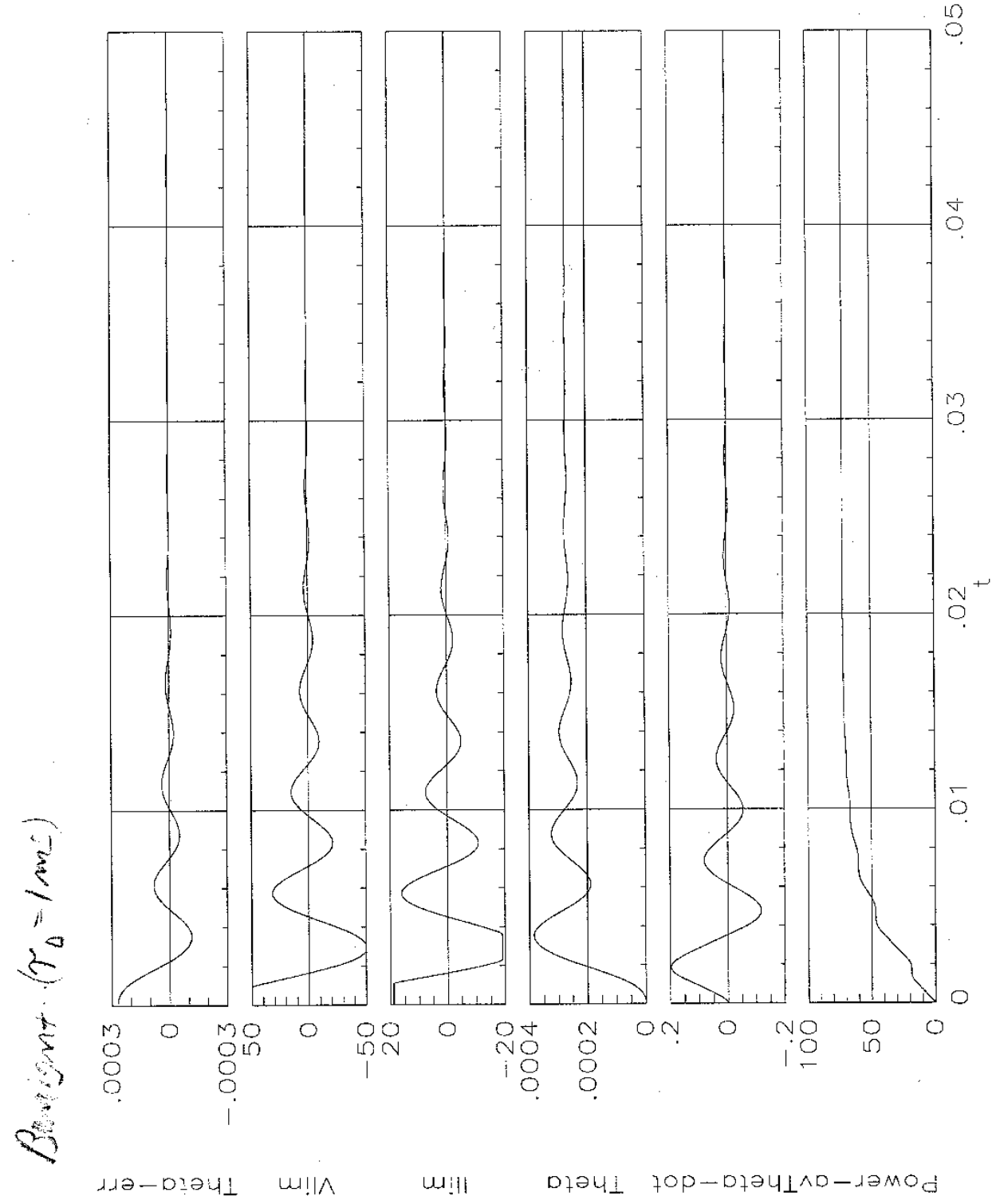
Power
avTheta-dot
Theta
Vlim
Ilim
Theta-err
.0003
0
-.0003
50
0
-50
-20
0
-20
.0004
.0002
0
.2
0
-.2
100
50
0
0
.01
.02
.03
.04
.05
t

Figure 18

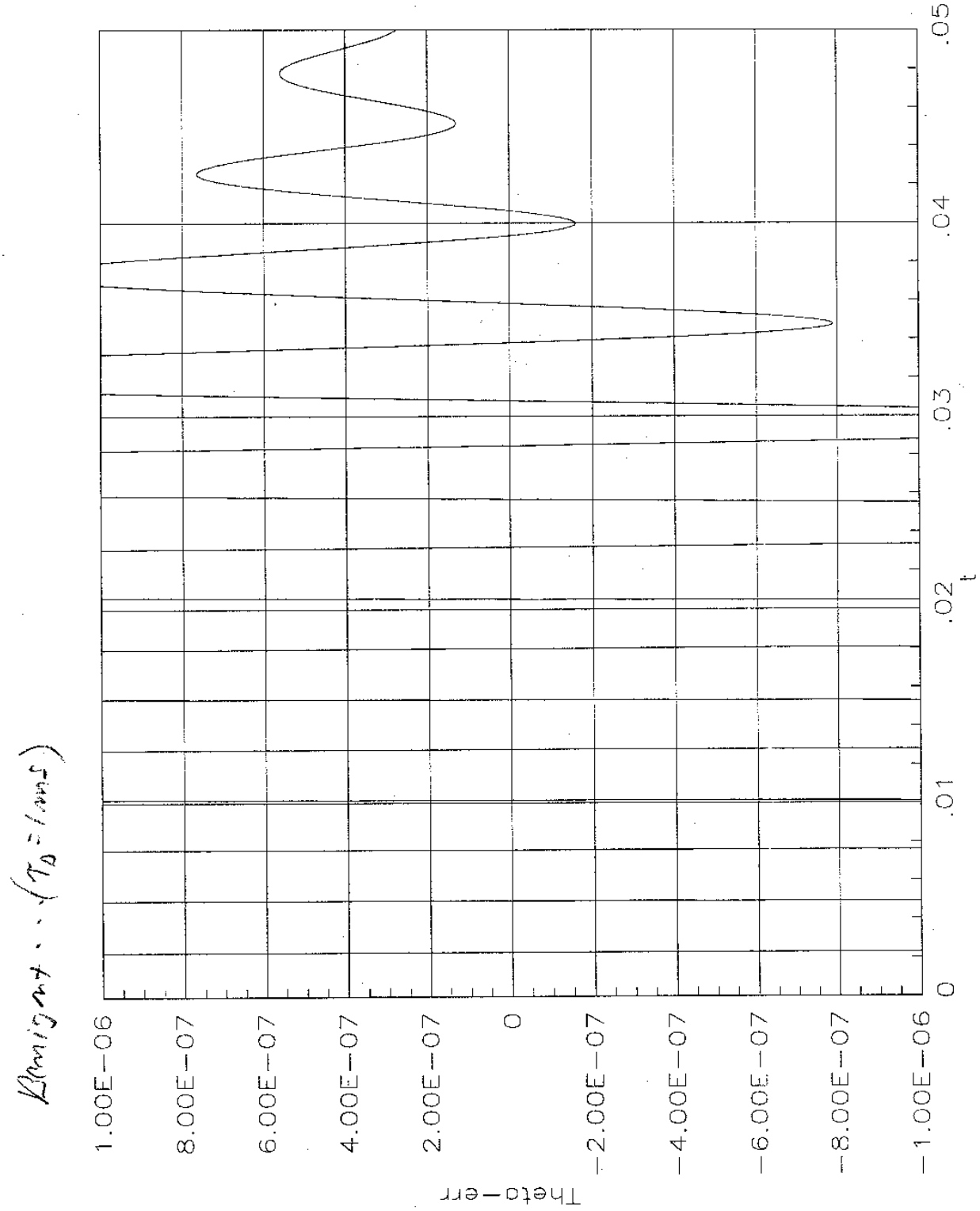
Theta—err
1.00E—06
8.00E—07
6.00E—07
4.00E—07
2.00E—07
0
—2.00E—07
—4.00E—07
—6.00E—07
—8.00E—07
—1.00E—06
0
.01
.02
.03
.04
.05
t

Figure 19

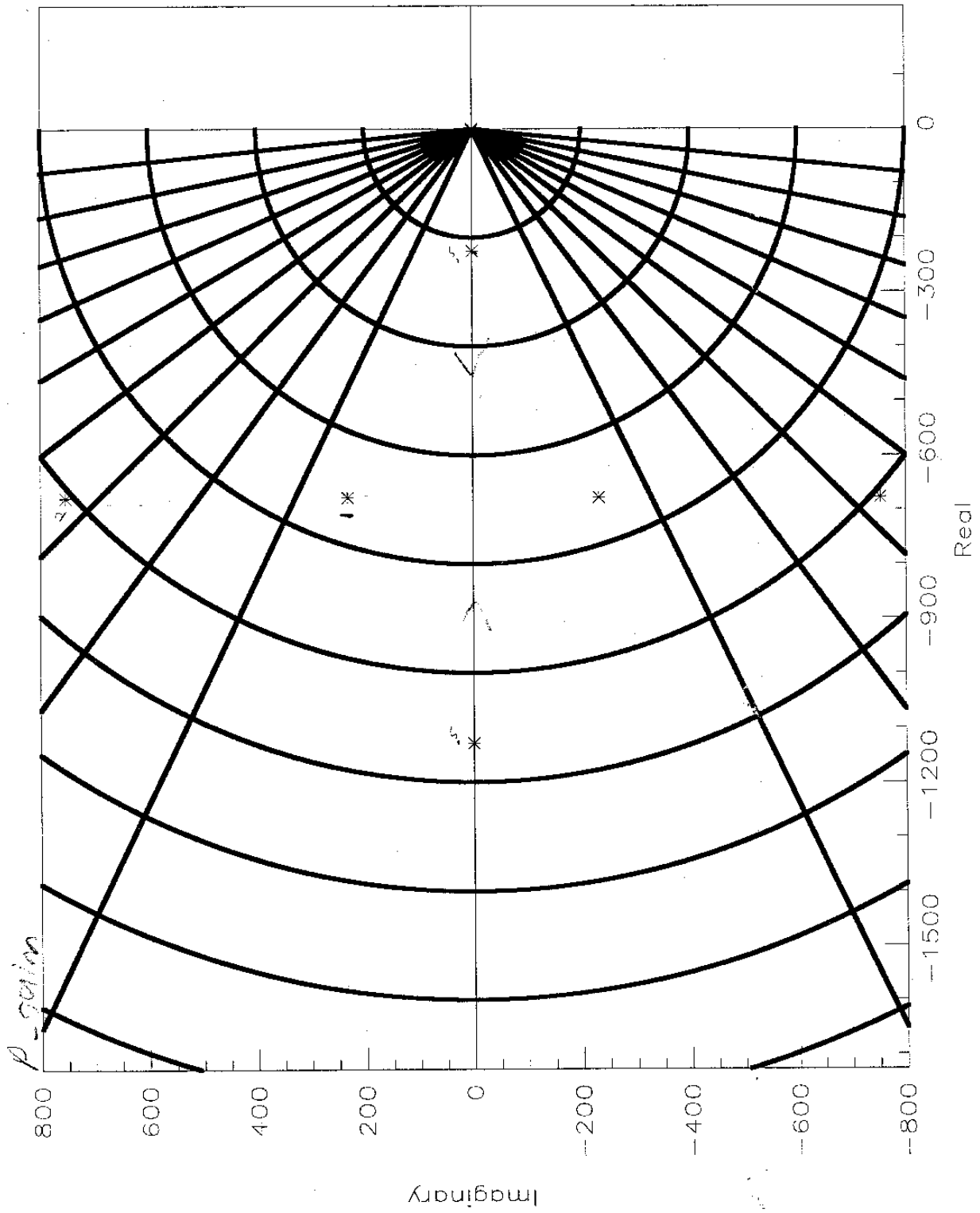
0
-300
-600
-900
-1200
-1500
Real
800
600
400
200
0
-200
-400
-600
-800
Imaginary

Figure 20

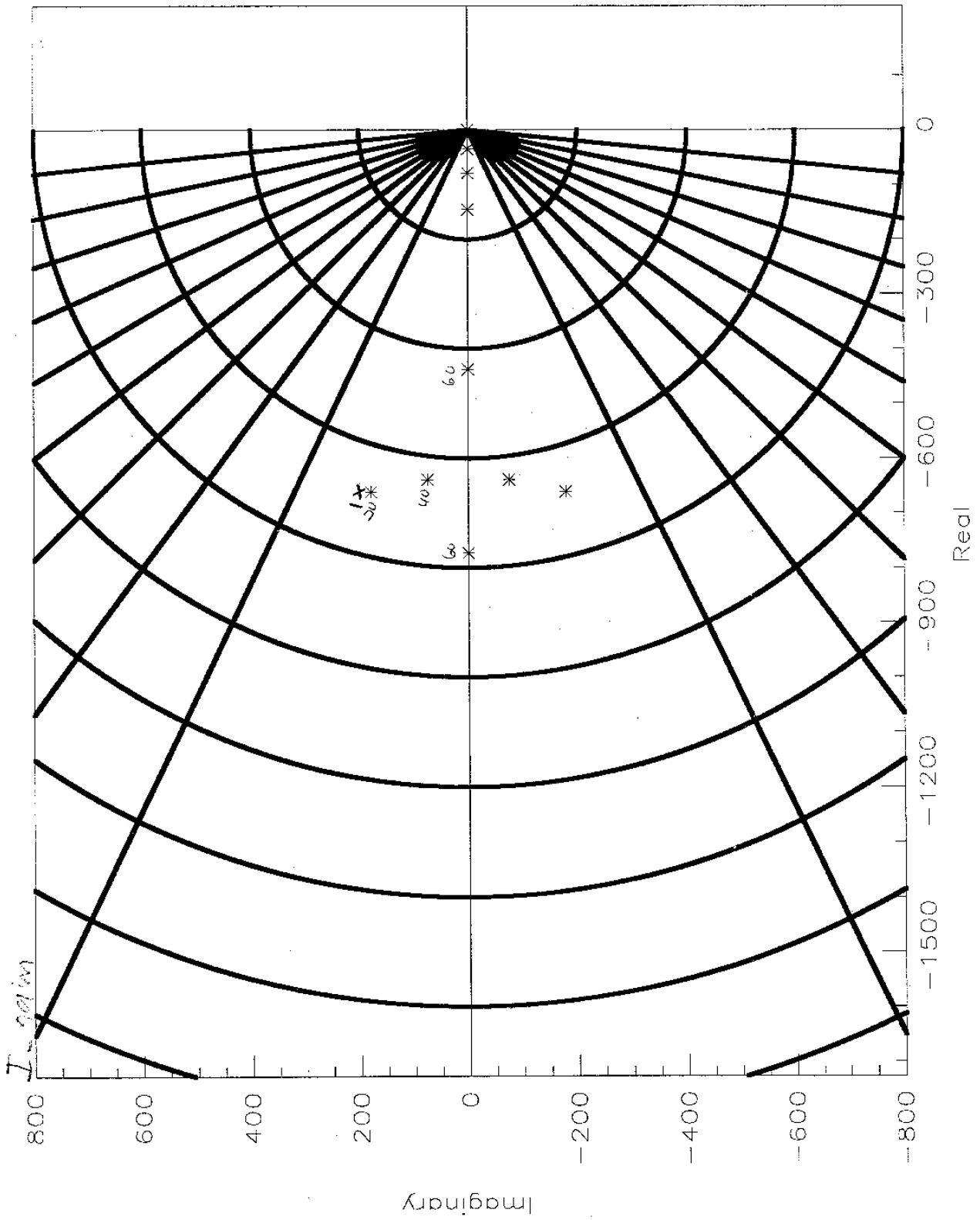
0
-300
-600
-900
-1200
-1500
Real
800
600
400
200
0
-200
-400
-600
-800
Imaginary

Figure 21

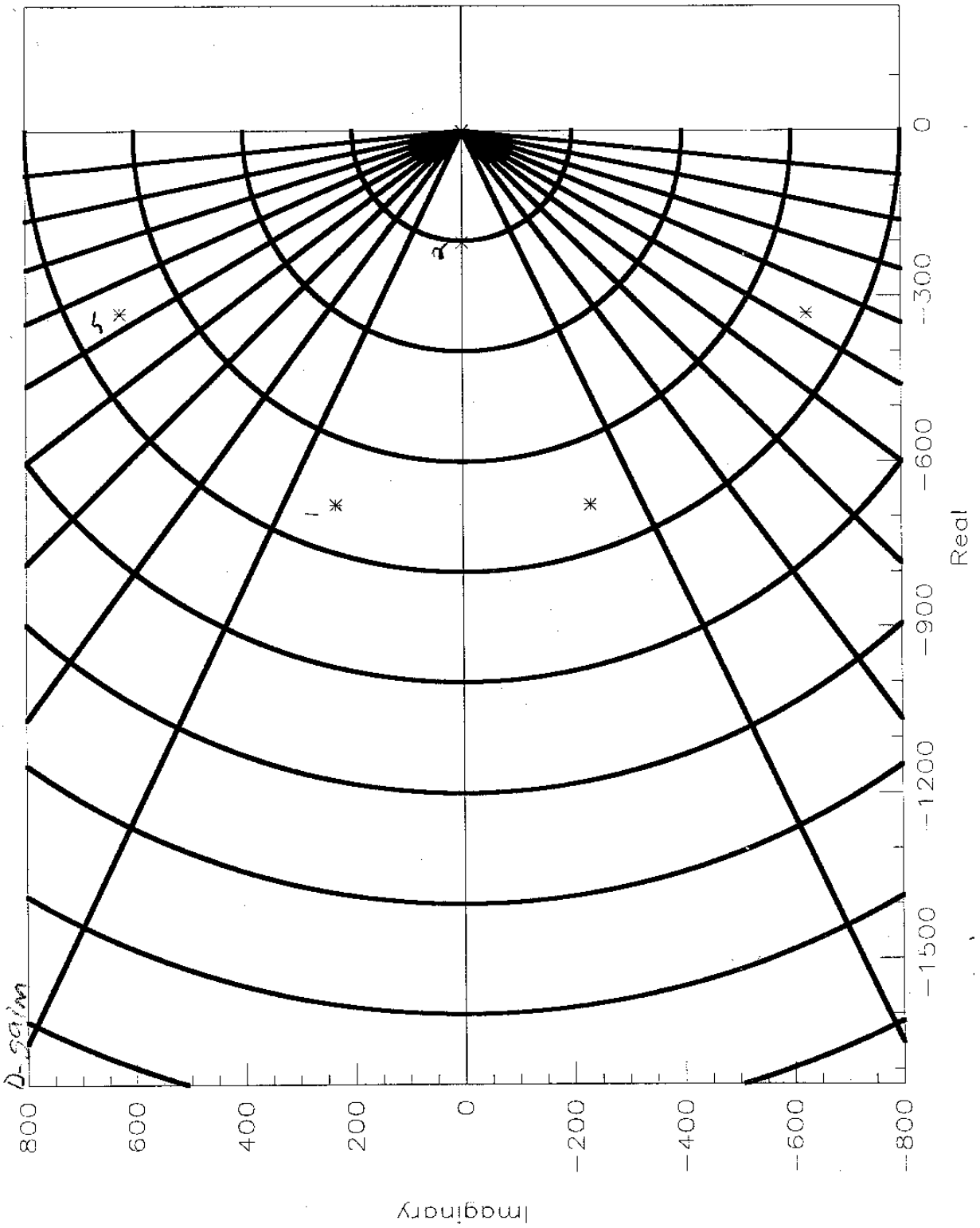
0
-300
-600
-900
-1200
-1500
Real
800
600
400
200
0
-200
-400
-600
-800
Imaginary

Figure 22

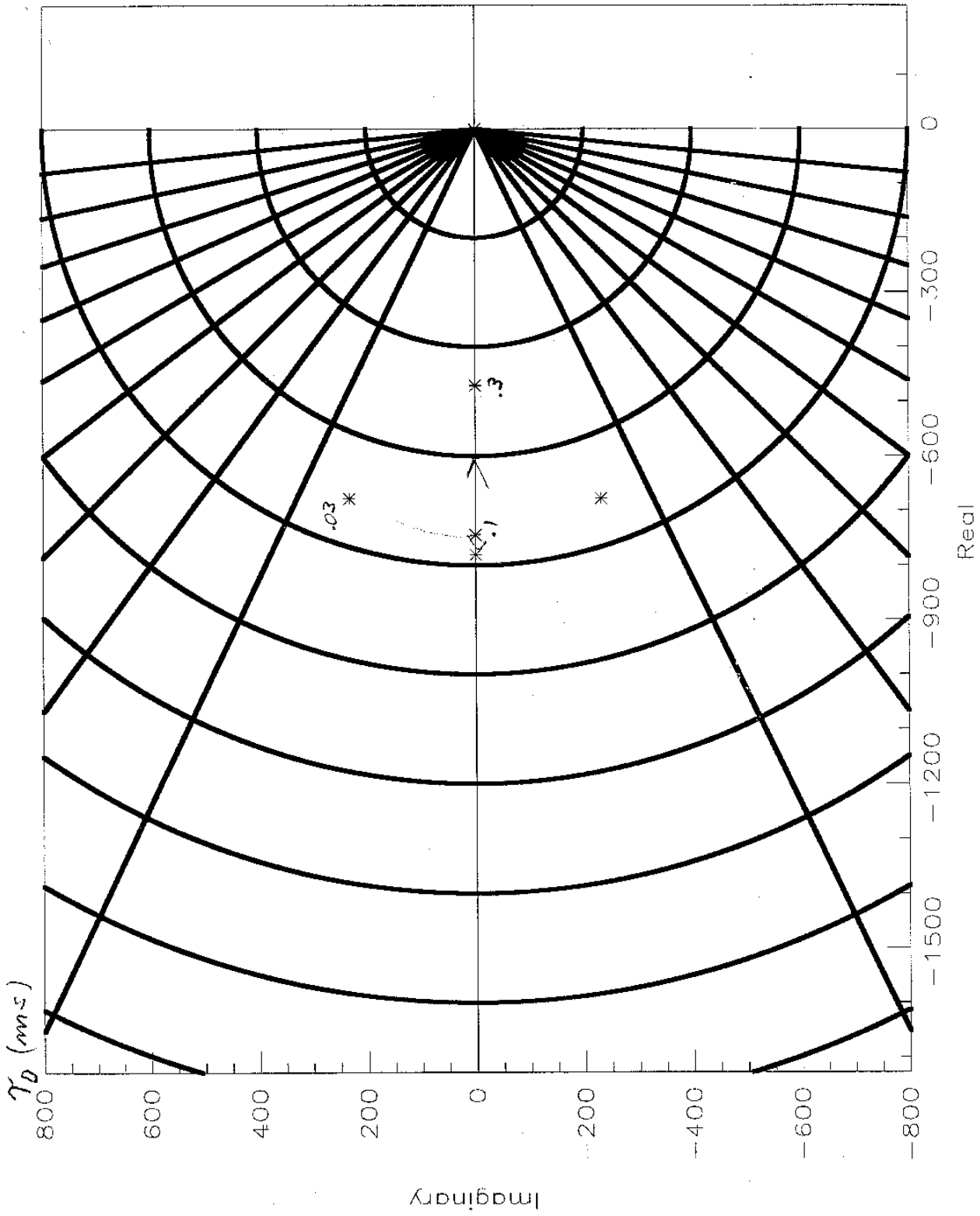
Real
0
-300
-600
-900
-1200
-1500
Imaginary
800
600
400
200
0
-200
-400
-600
-800
γ_D (nm^2)

Figure 23

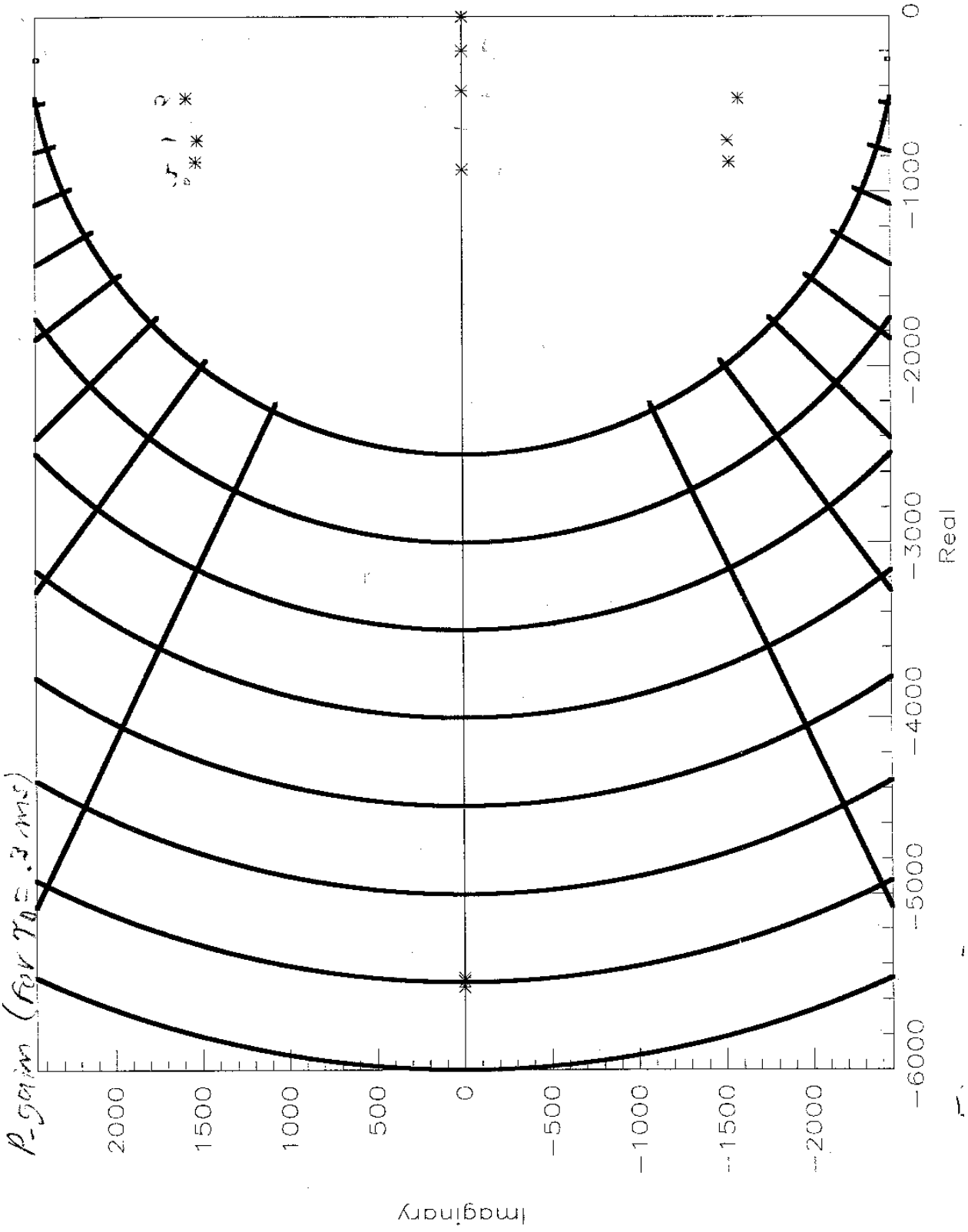
0
-1000
-2000
-3000
-4000
-5000
-6000
Real
2000
1500
1000
500
0
-500
-1000
-1500
-2000
Imaginary

Figure 24

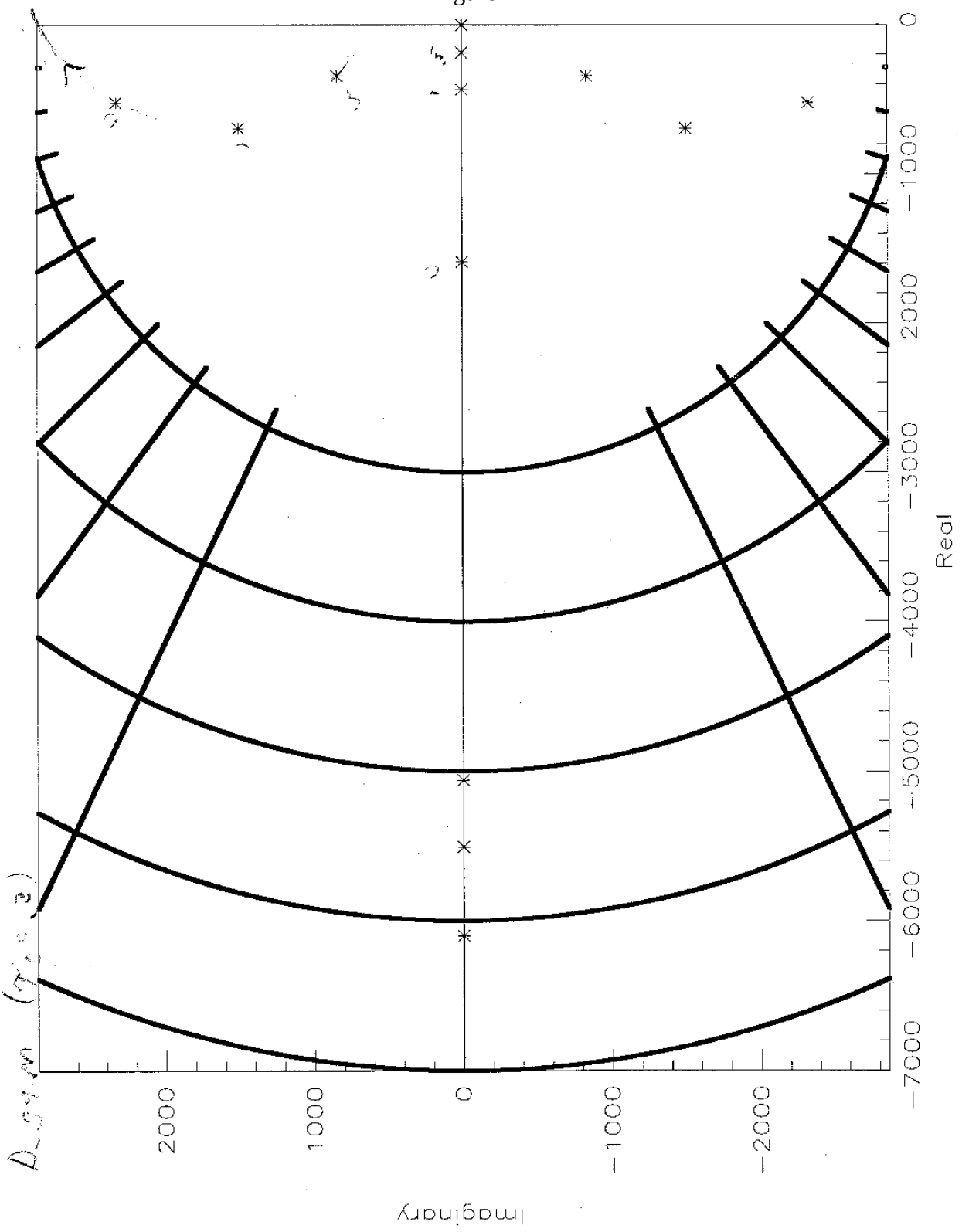
Real
0
-1000
-2000
-3000
-4000
-5000
-6000
-7000
Imaginary
2000
1000
0
-1000
-2000

Figure 25

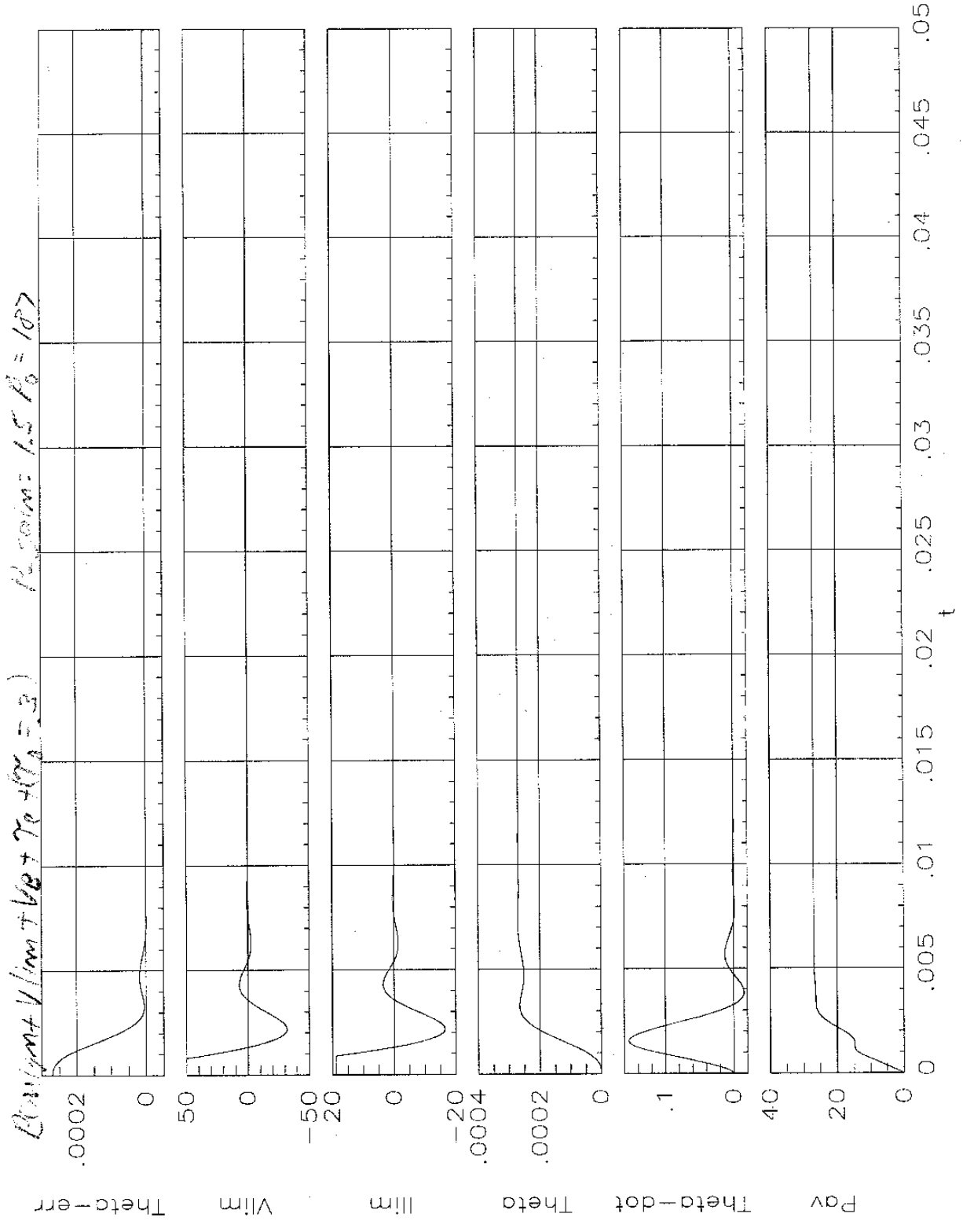
Theta_err
Vlim
Ilim
Theta
Theta_dot
Pav
t
0
.005
.01
.015
.02
.025
.03
.035
.04
.045
.05

Figure 26

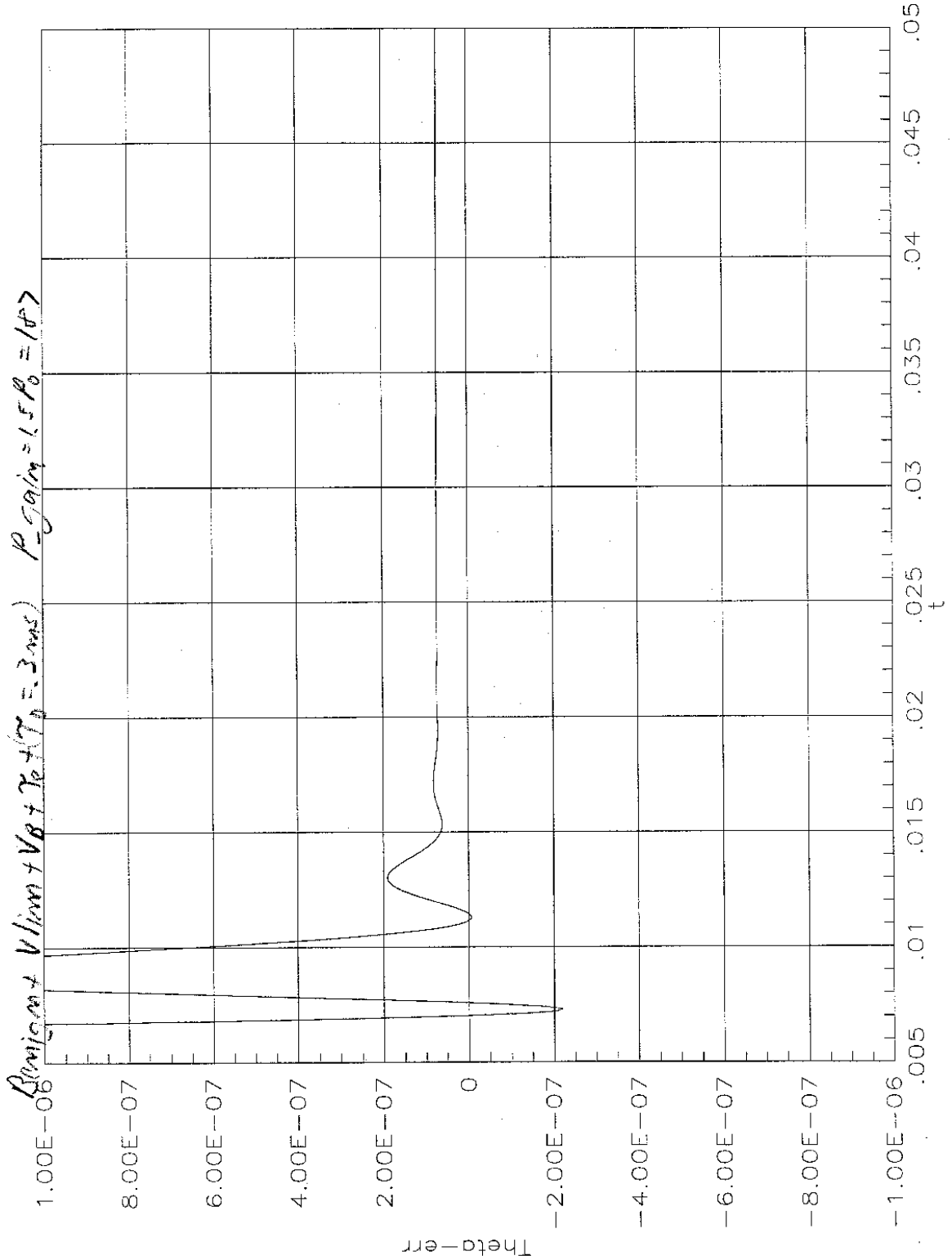
1.00E-06
8.00E-07
6.00E-07
4.00E-07
2.00E-07
0
-2.00E-07
-4.00E-07
-6.00E-07
-8.00E-07
-1.00E-06
Theta_err
.005
.01
.015
.02
.025
.03
.035
.04
.045
.05
t

Figure 27

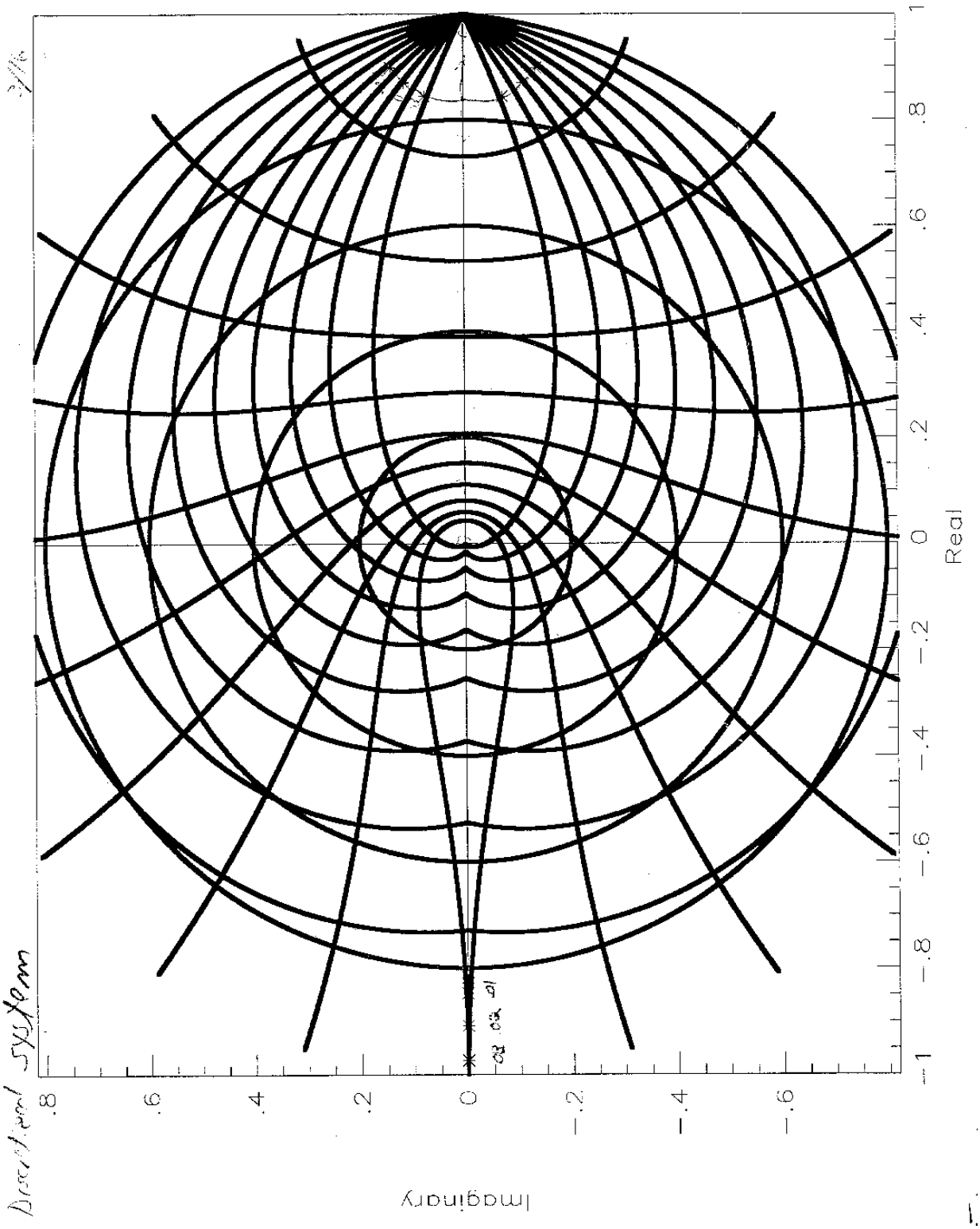

Figure 28

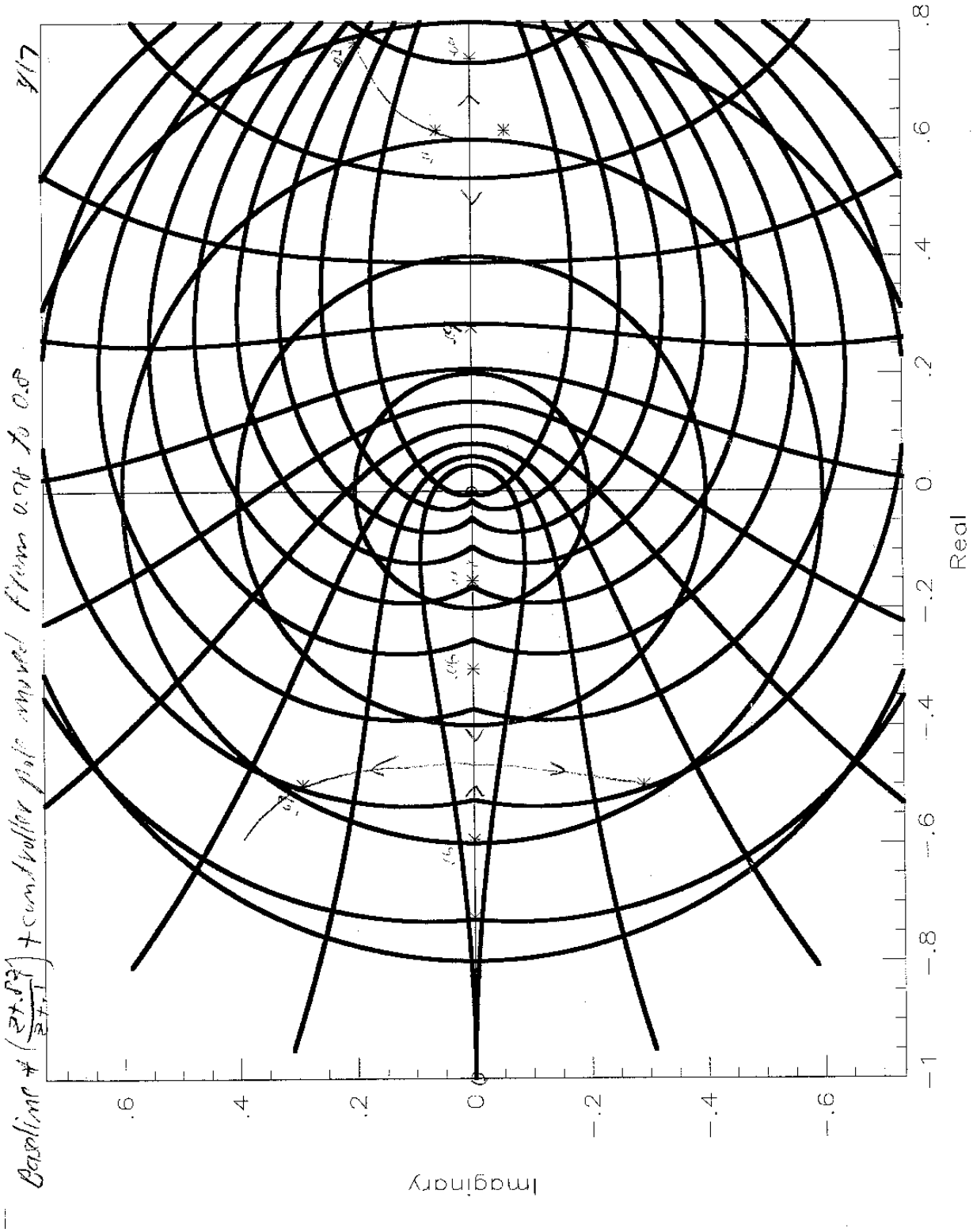

Figure 29

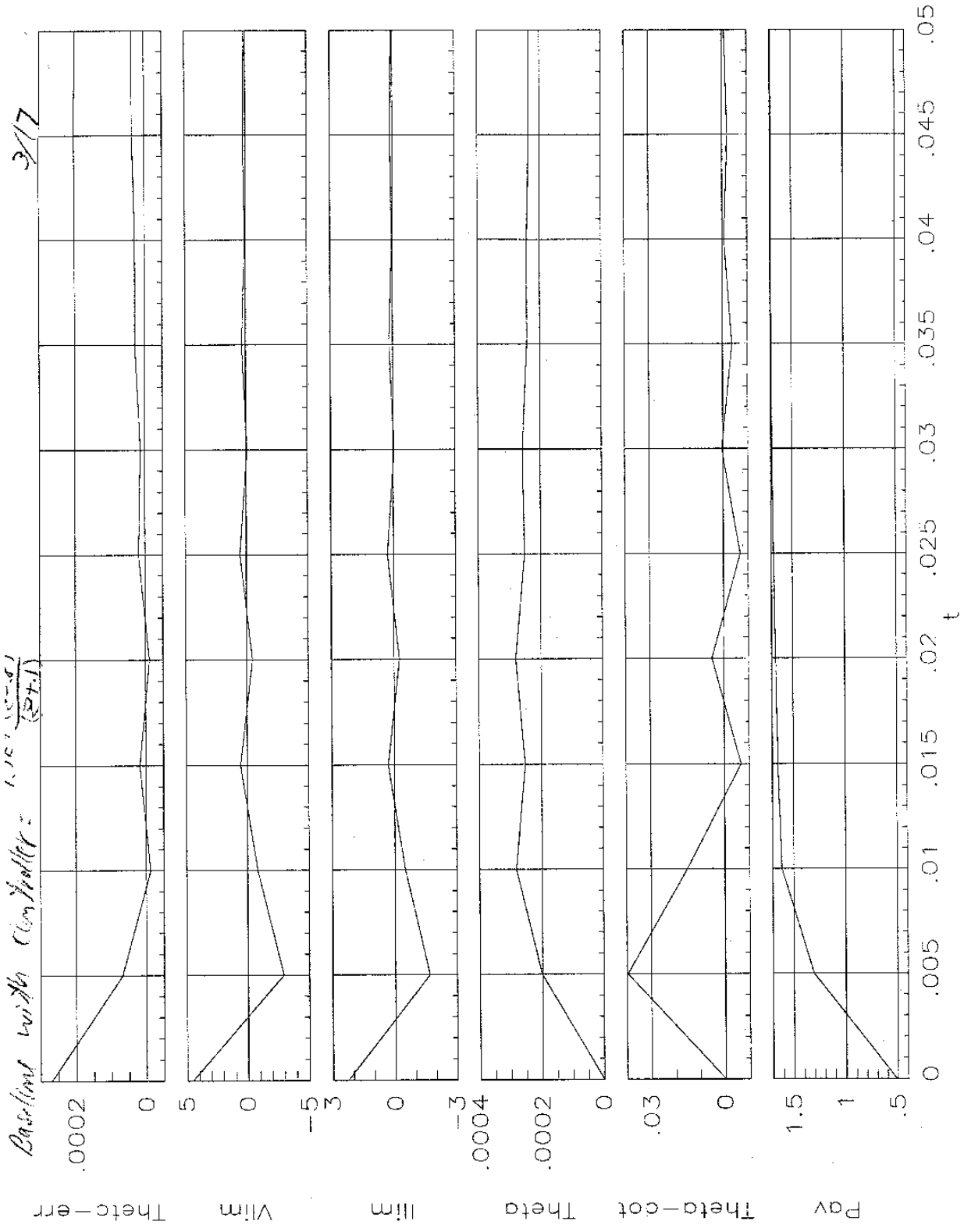
Theta_err
Vlim
Ilim
Theta
Theta_dot
Pav
t
0
.005
.01
.015
.02
.025
.03
.035
.04
.045
.05
.0002
0
5
0
−5
3
0
−3
.0004
.0002
0
.03
0
1.5
1
.5

Figure 30

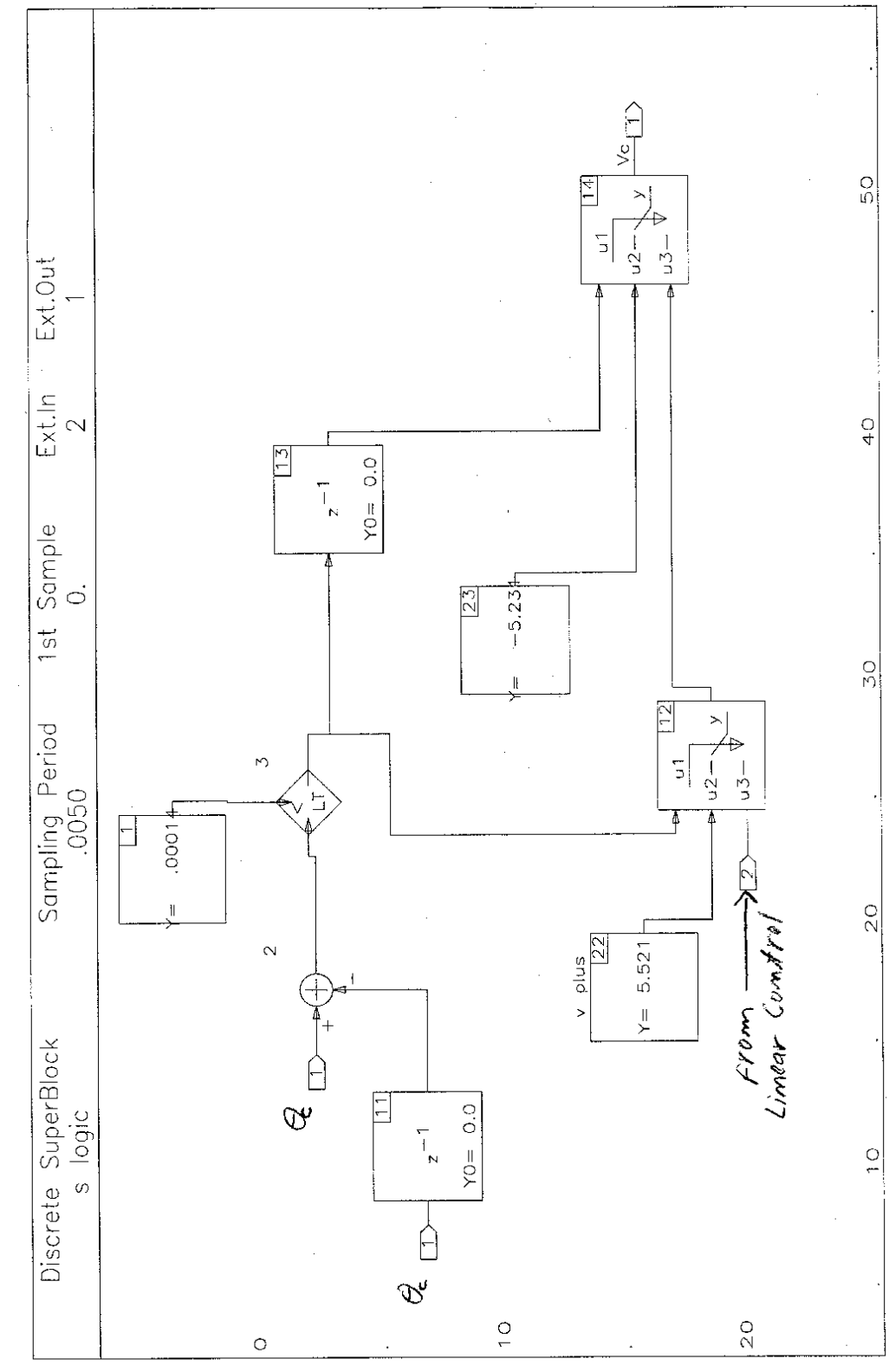
Discrete SuperBlock
s logic
Sampling Period
.0050
1st Sample
0.
Ext.In
2
Ext.Out
1
Y= .0001
LT
z-1
YO= 0.0
Y= -5.231
u1
u2
u3
y
Vc
v plus
Y= 5.521
From Linear Control
0
10
20
30
40
50

Figure 31

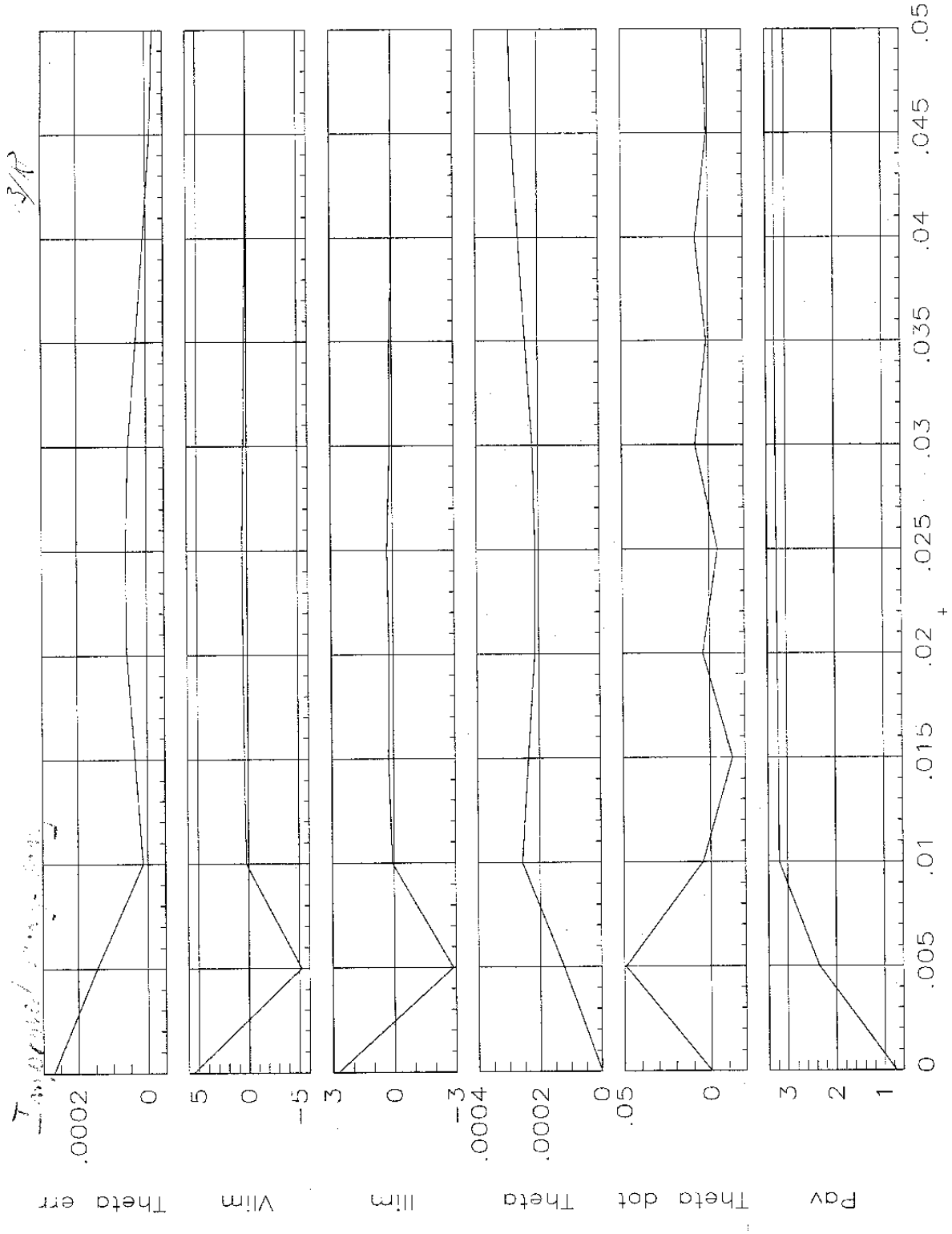
Theta err
.0002
0
Vlim
5
0
−5
Ilim
3
0
−3
Theta
.0004
.0002
0
Theta dot
.05
0
Pav
3
2
1
0
.005
.01
.015
.02
.025
.03
.035
.04
.045
.05
t

Figure 32

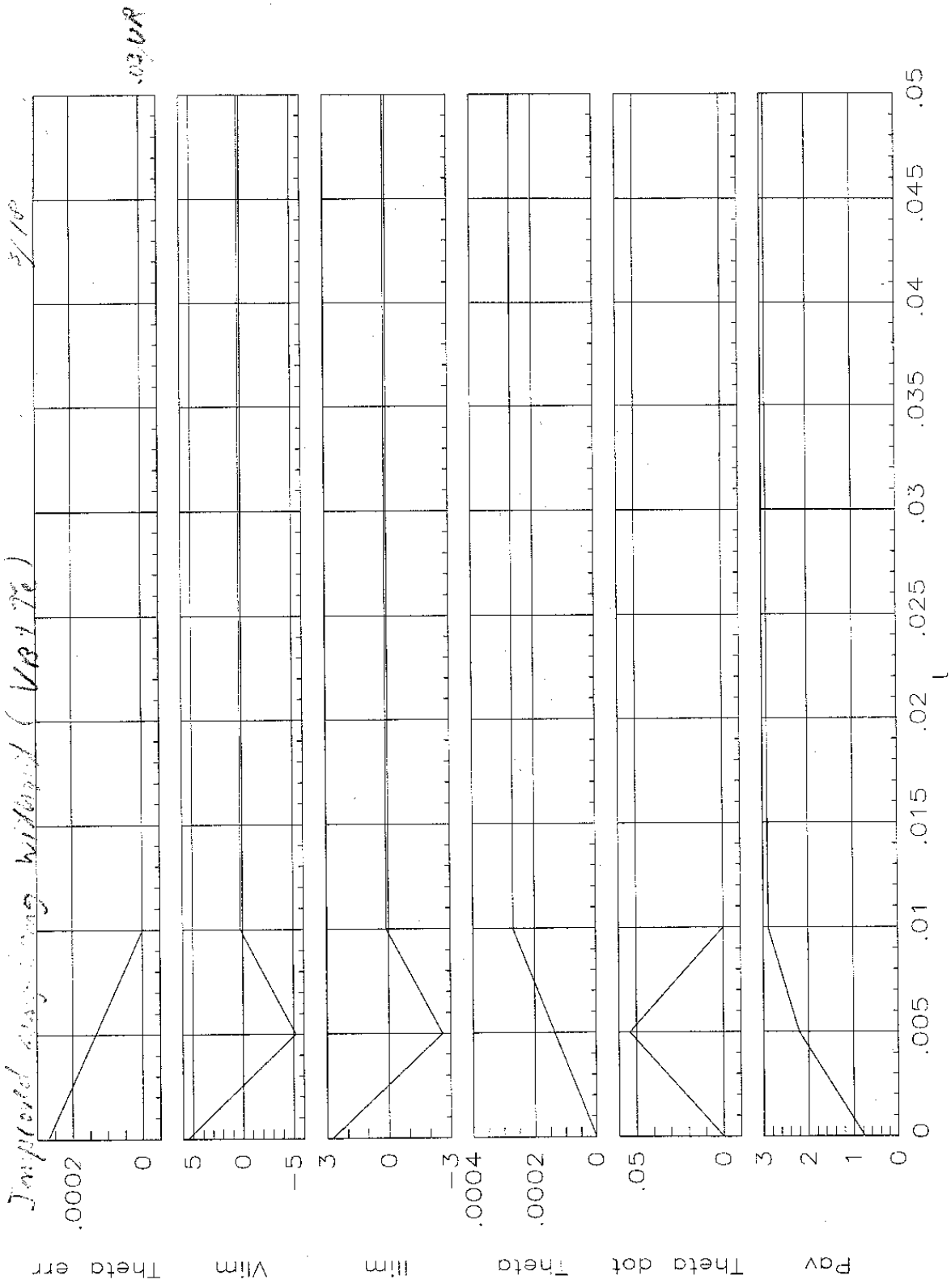
Theta err
Vlim
Ilim
Theta
Theta dot
Pav
.0002
0
5
0
−5
3
0
−3
.0004
.0002
0
.05
0
3
2
1
0
0
.005
.01
.015
.02
.025
.03
.035
.04
.045
.05
t

Figure 33

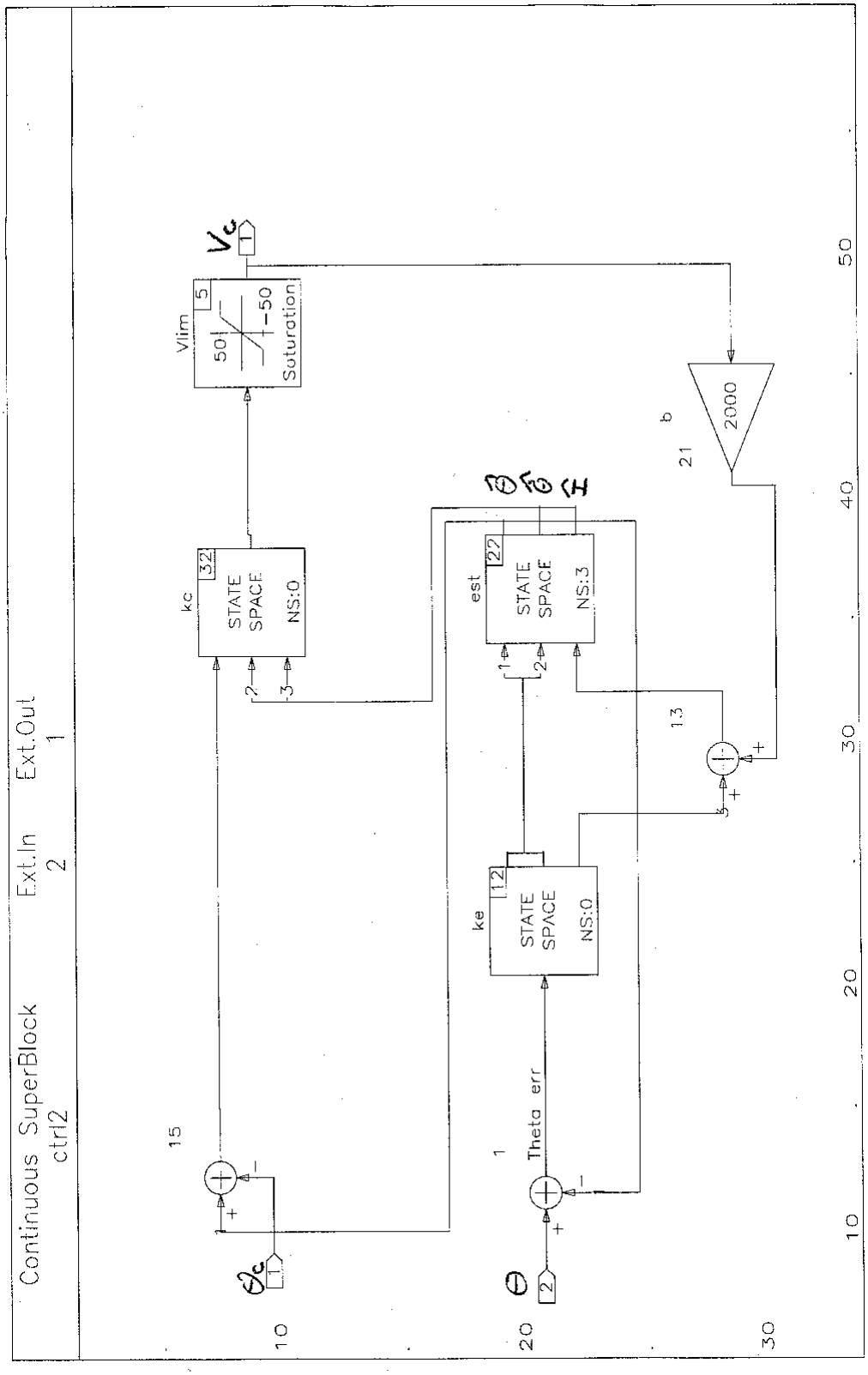
Continuous SuperBlock
ctrl2
Ext.In
2
Ext.Out
1
Vc
1
Vlim
5
50
-50
Saturation
kc
32
STATE SPACE
NS:0
est
22
STATE SPACE
NS:3
ke
12
STATE SPACE
NS:0
b
21
2000
15
13
1
Theta err
θc
1
θ
2
10
20
30
40
50

Figure 34

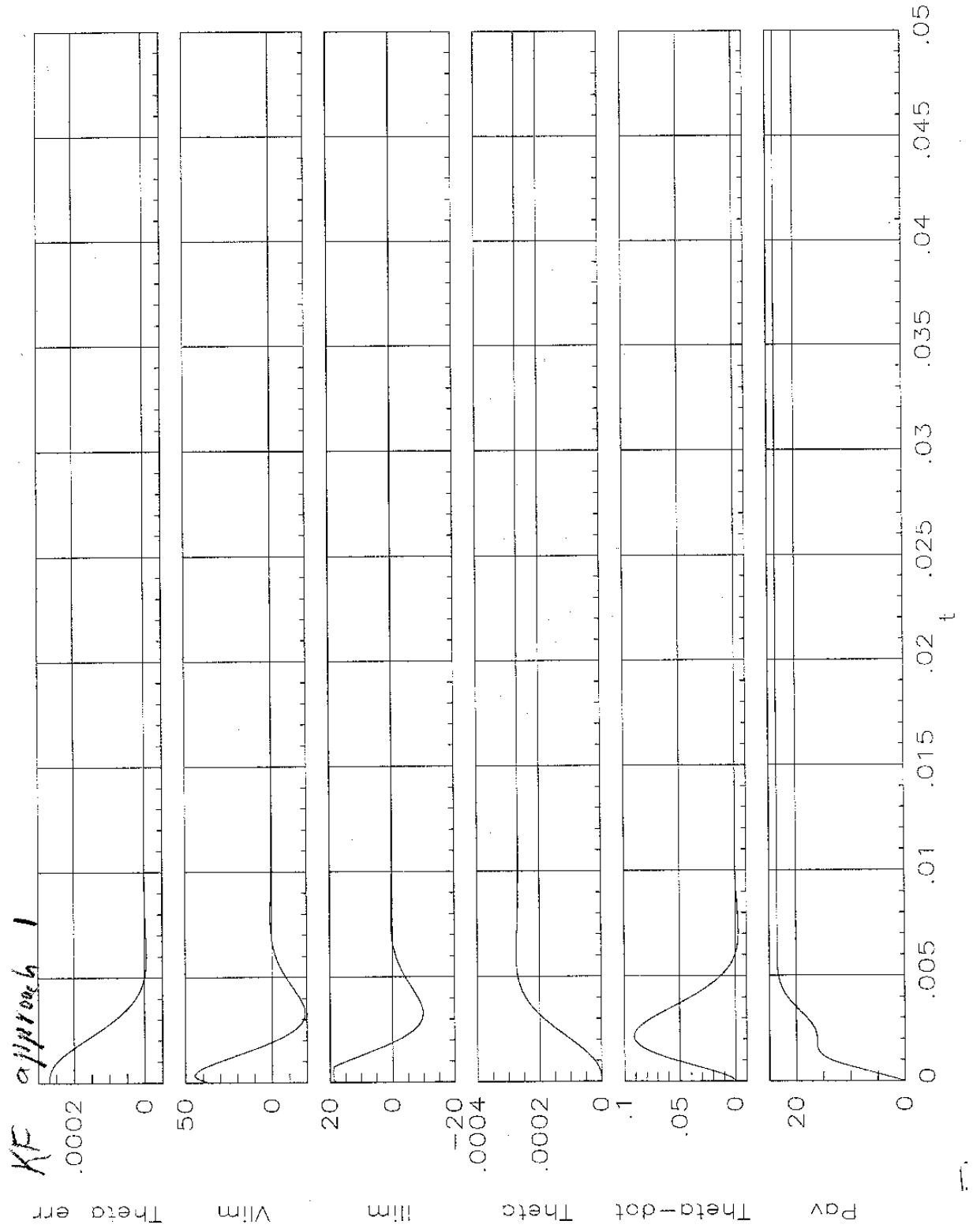
KE
Theta err
.0002
0
Vlim
50
0
ilim
20
0
Thetc
−20
.0004
.0002
0
Theta−dot
.1
.05
0
Pav
20
0
0
.005
.01
.015
.02
.025
.03
.035
.04
.045
.05
t

Figure 35

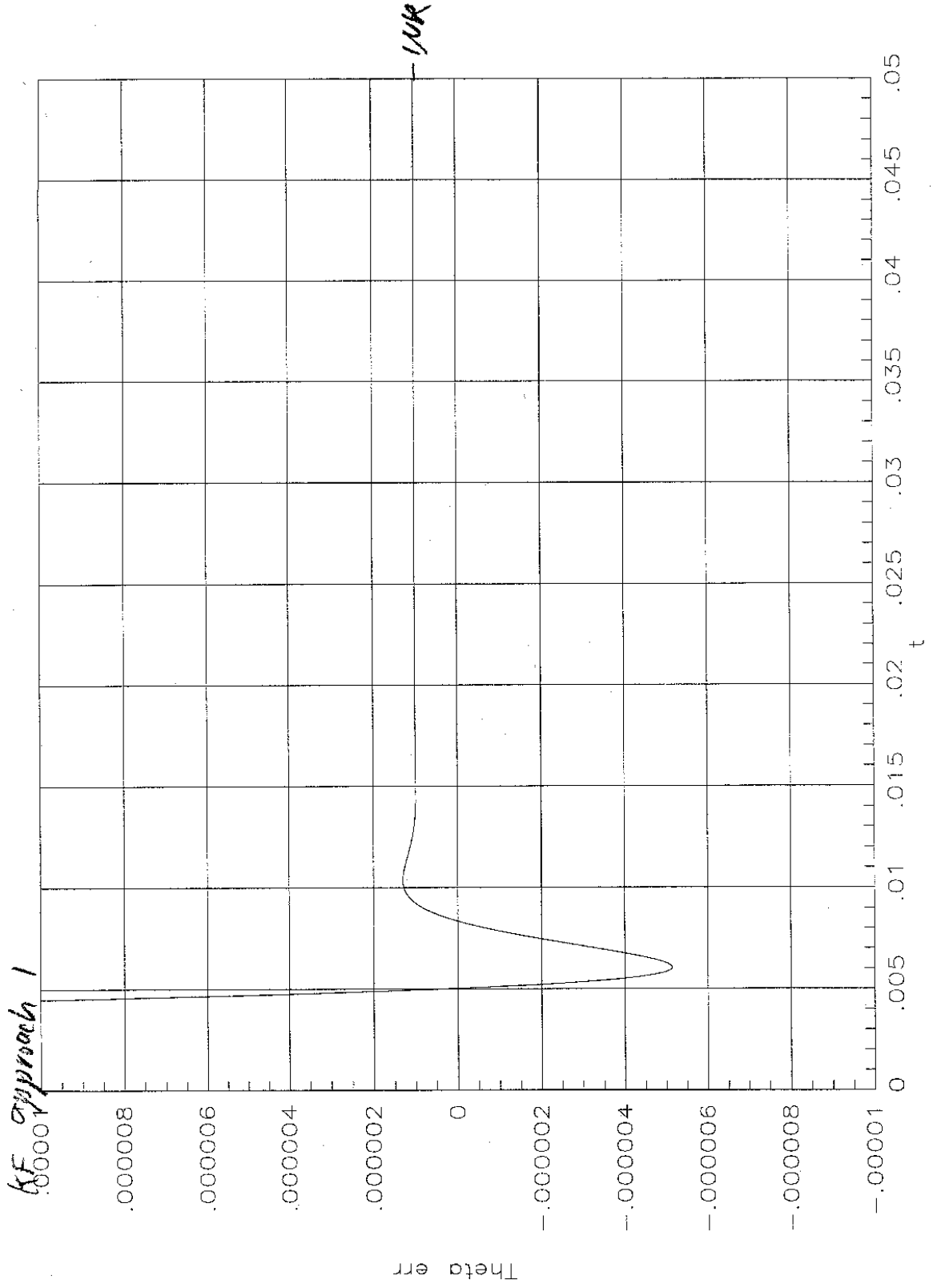
INR
KF approach 1
Theta err
.00001
.000008
.000006
.000004
.000002
0
-.000002
-.000004
-.000006
-.000008
-.00001
0
.005
.01
.015
.02
.025
.03
.035
.04
.045
.05
t

Figure 36

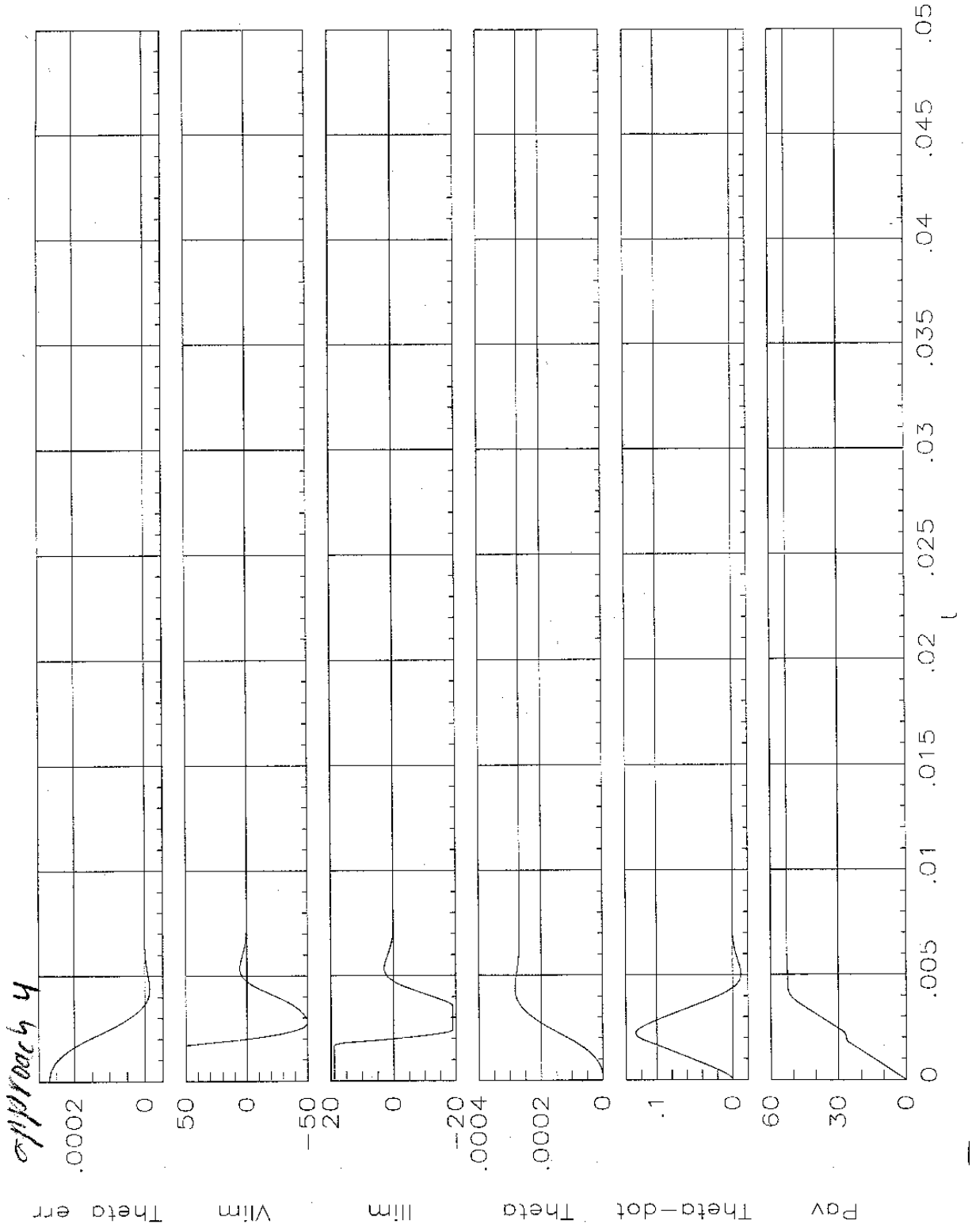
Theta err
Vlm
Ilm
Theta
Theta-dot
Pav
.0002
0
50
0
-50
-20
0
-20
.0004
.0002
0
.1
0
60
30
0
0
.005
.01
.015
.02
.025
.03
.035
.04
.045
.05
t

Figure 37

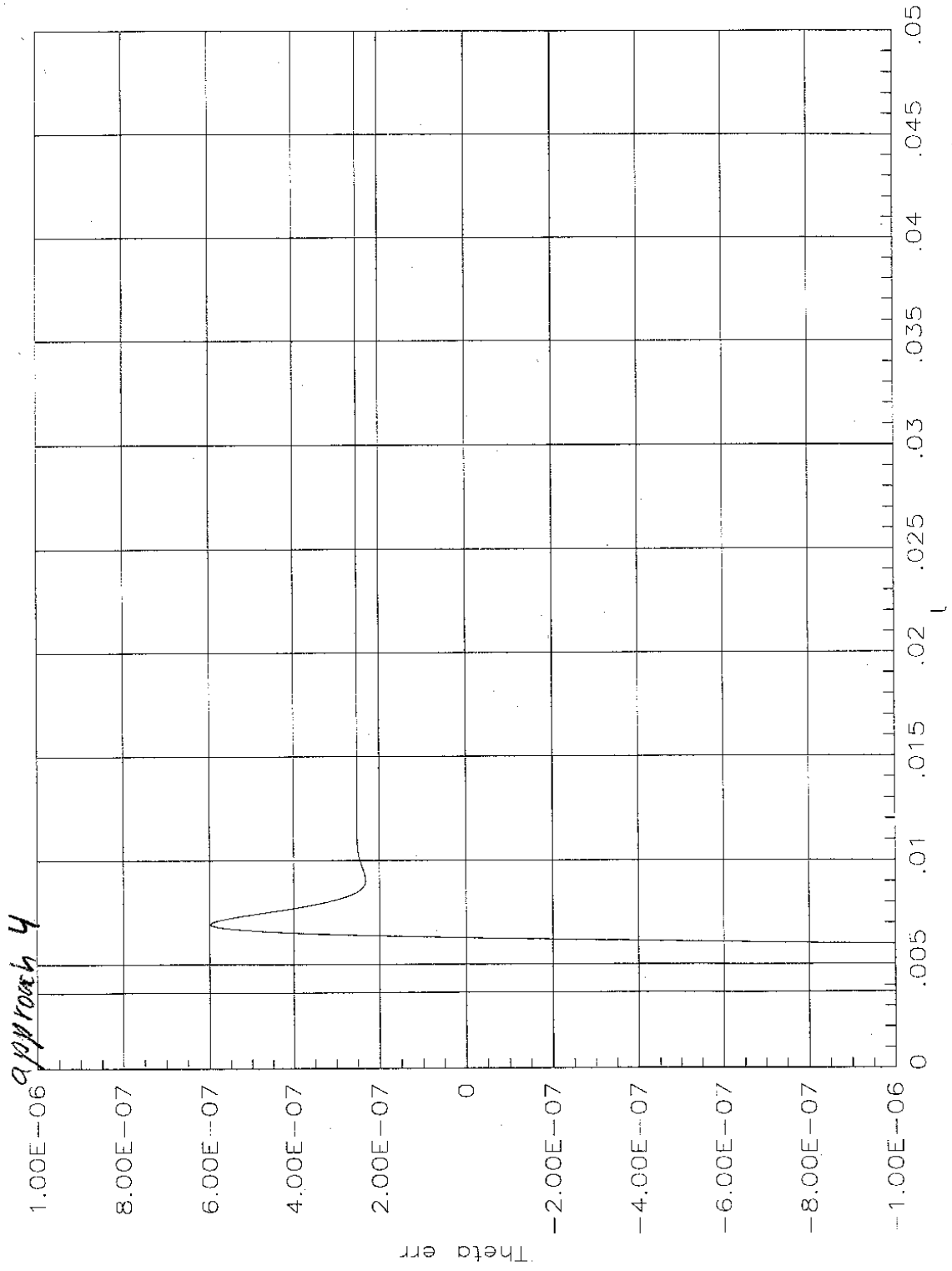
approach 4
Theta err
L
1.00E-06
8.00E-07
6.00E-07
4.00E-07
2.00E-07
0
-2.00E-07
-4.00E-07
-6.00E-07
-8.00E-07
-1.00E-06
0
.005
.01
.015
.02
.025
.03
.035
.04
.045
.05

Figure 38

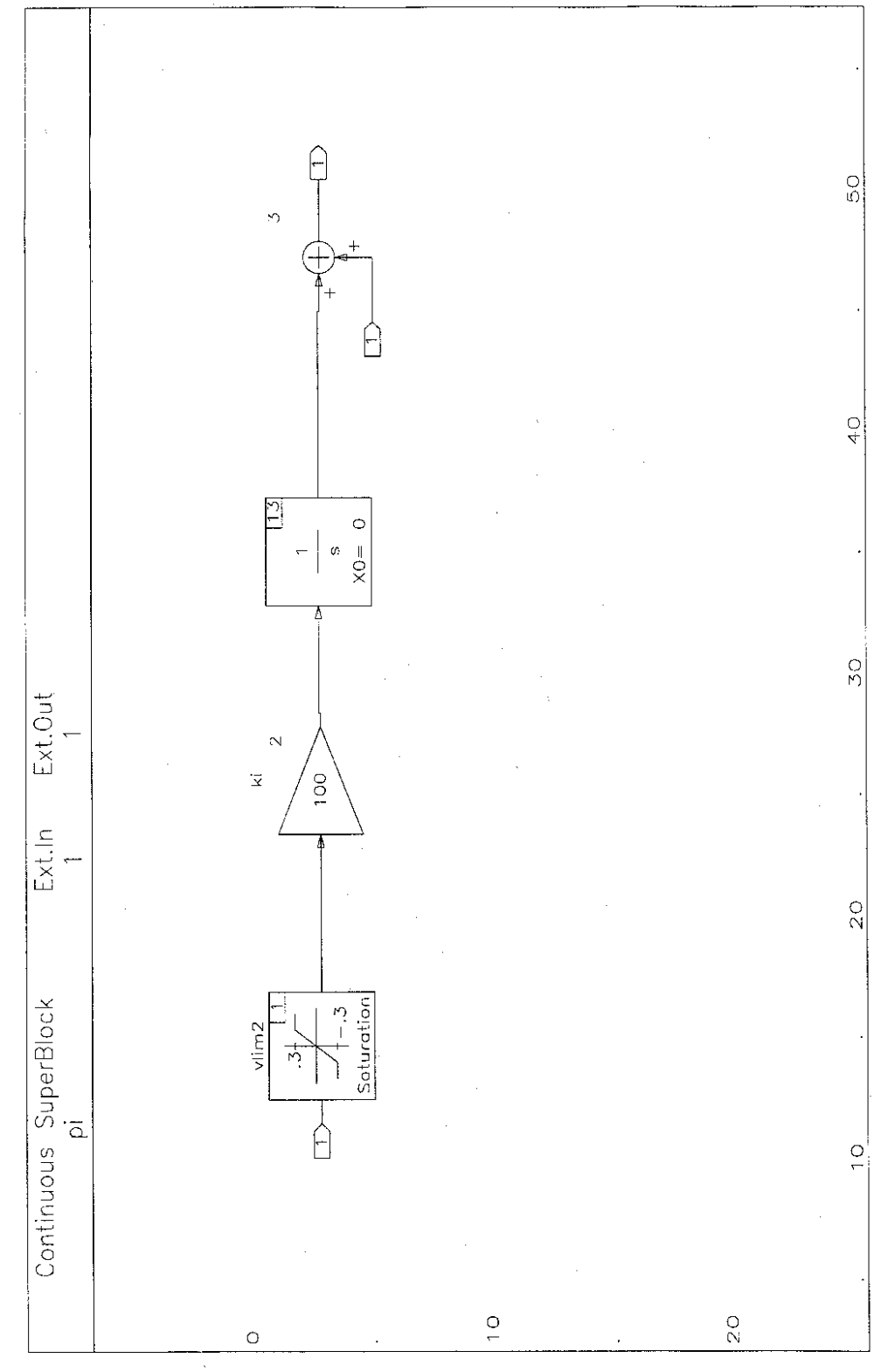
Continuous SuperBlock
pi
Ext.In 1
Ext.Out 1
vlim2
.3
-.3
Saturation
ki
2
100
1.3
1
s
X0= 0
3
+
+
1
1
1
0
10
20
10
20
30
40
50

Figure 39

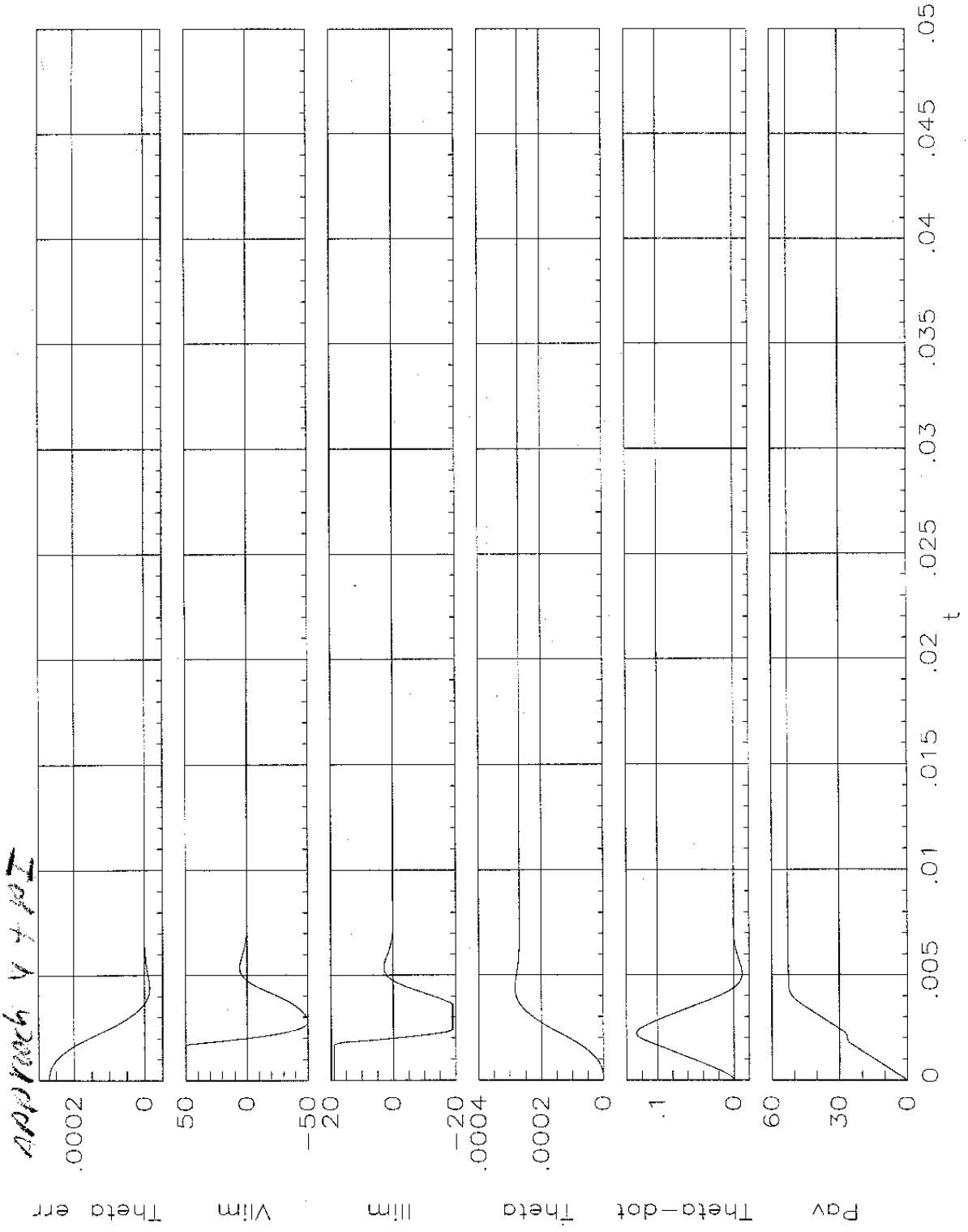
Theta err
Vlim
Ilim
Theta
Theta-dot
Pav
.0002
0
50
0
−50
−20
0
−20
.0004
.0002
0
.1
0
60
30
0
0
.005
.01
.015
.02
.025
.03
.035
.04
.045
.05
t

Figure 40

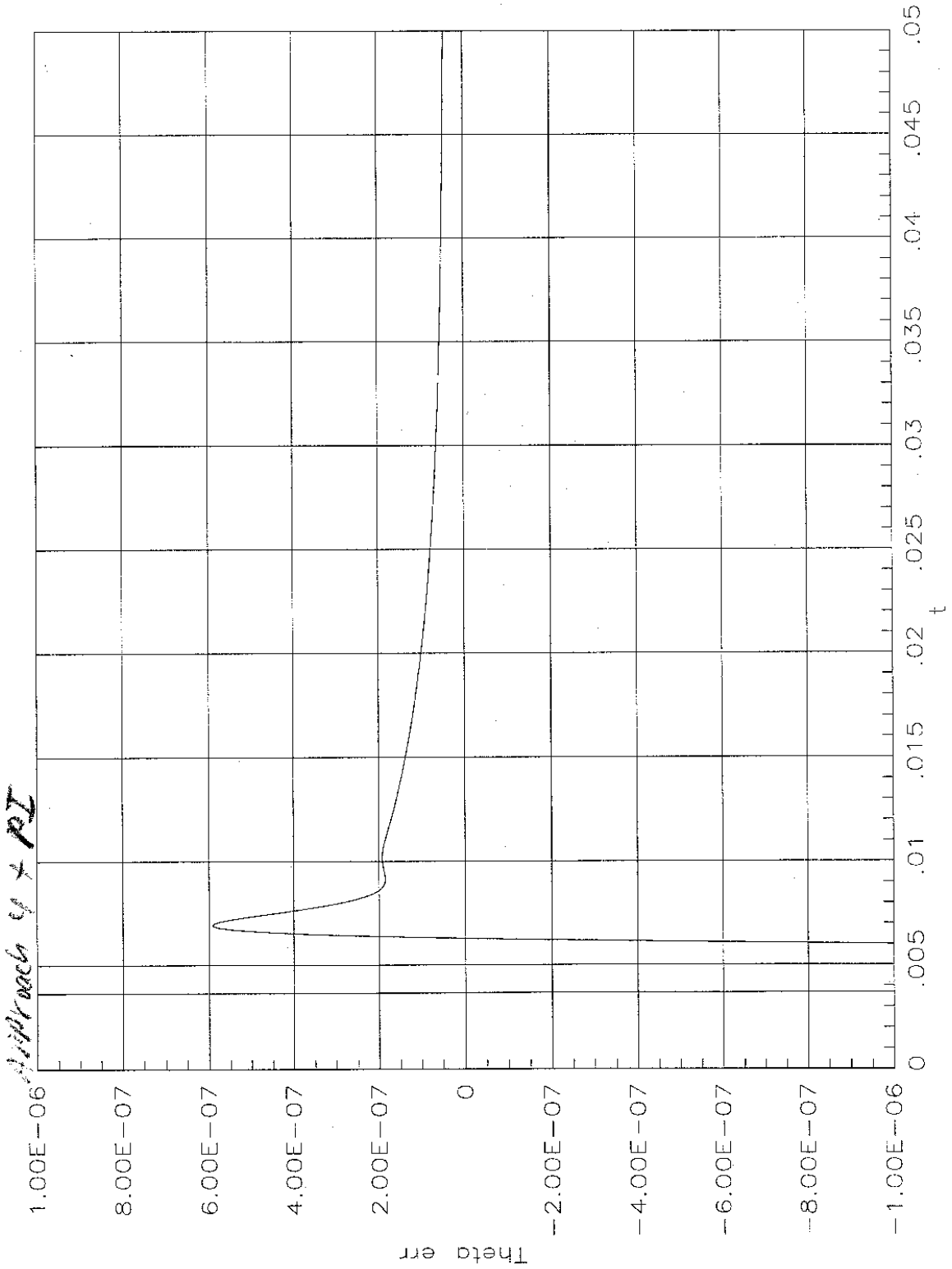
Theta err
1.00E-06
8.00E-07
6.00E-07
4.00E-07
2.00E-07
0
-2.00E-07
-4.00E-07
-6.00E-07
-8.00E-07
-1.00E-06
0
.005
.01
.015
.02
.025
.03
.035
.04
.045
.05
t